Chapter 6

Accelerator Technologies

6.1 Magnets

L. BOTTURA, F. BOATTINI, B. BORDINI, M. BRESCHI, B. CAIFFI, S. FABBRI, S. MARIOTTO, A. PORTONE, M. STATERA, IMPORTANT NOTE: *TO BE COMPLETED AFTER DISCUSSION AT THE MMWG*

Introduction

The Muon Collider poses extraordinary challenges to magnet technology, and meeting them will benefit not only the most efficient accelerator at the energy frontier, but also several other fields of science and societal applications. Through the integrated study and conceptual design activities of the last three years (2022-2024) we have identified the following grand challenges that have driven magnet R&D activities:

- Steady state superconducting solenoids for
- Target, decay and capture channel
- 6D cooling channel
- Final cooling channel
- Fast pulsed normal conducting magnet systems, including the power converter and management, for the rapid cycled synchrotrons
- Steady state superconducting accelerator magnets, dipoles, quadrupoles and combined functions, for the rapid cycled synchrotrons and collider arc and interaction region.

The sections below describe the main achievements of the work performed in the period since the last Strategy Upgrade, in 2021. We provide in particular a description of the concepts selected, the details of the engineering design and supporting analysis, an evaluation of the challenges to magnet technology, and a reasoned summary of target performance for on-going and future developments.

Target, decay and capture channel solenoid

Magnet design and engineering

The solenoids that host the target and capture channel, where the muon beam is produced, pose the first grand challenge. The magnetic field profile along the axis of the channel has a shape derived from studies of optimal generation and capture, with peak field of 20 T on the target, and a decay to approximately 1.5 T at the exit of the channel, over a total length of approximately 18 m. The characteristic length of the field change is about 2.5 m, i.e. much larger than the gyration radius of the muons in the field so that the beam expands adiabatically in the channel. Such field profile can be generated

The interaction of the proton beam with the target produces a considerable amount of radiation, which needs heavy shielding to avoid heating and damaging the materials of the superconducting coils

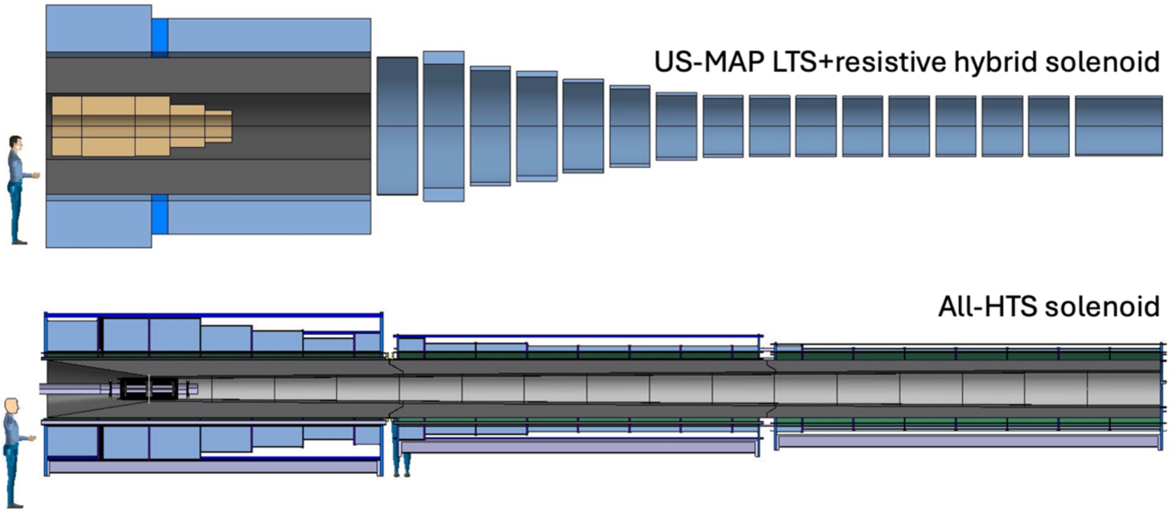

Fig. 6.1.1: Comparison (to scale) of the solenoid coils of the target, decay and capture channel of a Muon Collider, as produced by the MAP study (top) [294] and resulting from the optimization of an all-HTS solution (bottom) [328]

of the target solenoid. A free bore of at least 1.4 m is necessary to host the nuclear shield around the target. Such large bore dimension result in high stored magnetic energy, which in turn affects magnet protection, and electromagnetic forces.

We have developed a fully superconducting solution for the 2 MW target variant, based on a HTS cable inspired by recent developments in the field of magnetically confined thermonuclear fusion. Field levels of 20 T are at the upper limit of performance for small bore Nb3Sn, and arguably out of reach for LTS with the bore dimension required. More important, the choice of HTS gives the possibility to set an operating point at a temperature higher than liquid helium. This brings the benefit of increased cryogenic efficiency, reduced wall-plug power consumption, and reduced helium inventory. We have set a reference an operating temperature in the range of 20 K, which has an efficiency advantage of a factor 5 with respect to cooling at liquid helium, 4.5 K.

The solution reached is shown in the schematic view of Fig. M1, contrasted to the design originally proposed by US-MAP [294]. Thanks to the choice of HTS, operated at high cryogenic temperature, the stored energy is reduced by a factor three from the US-MAP value of 3 GJ to 1.4 GJ of the present design, and the cold mass is similarly reduced by a factor two from the US-MAP value of 200 tons to about 100 tons of the present design. This has significant impact on system cost. In addition the elimination of the resistive insert in the US-MAP proposal, and operation at 20 K, yield to an estimated wall-plug power consumption below 1 MW, to be compared to the estimated 12 MW of the US-MAP proposal.

The reference configuration (December 2024) is reported in Tab. MI, where we give the details of the coil geometry, the number of turns and pancakes, and the operating current of each solenoid. To be noted that this configuration was obtained with equal current in all conductors (61.15 kA), the file profile being the result of the geometry optimization. This greatly simplifies powering and protection, allowing to have several of the low-field modules in series, thus reducing the number of circuits and the number of leads.

Solenoid Module	R_c (m)	Z_c (m)	DR (m)	D_z (m)	Turns (-)	Pancakes (-)	I_{coil} (MA-turn)
SC1	0.970	-1.185	0.540	0.830	13	20	15.899
SC2	0.970	-0.335	0.540	0.830	13	20	15.899
SC3	0.970	0.515	0.540	0.830	13	20	15.899
SC4	0.887	1.365	0.374	0.830	9	20	11.007
SC5	0.825	2.215	0.249	0.830	6	20	7.338
SC6	0.783	3.065	0.166	0.830	4	20	4.892
SC7	0.825	3.708	0.249	0.415	6	10	3.669
SC8	0.704	4.603	0.208	0.415	5	10	3.058
SC9	0.642	5.245	0.083	0.830	2	20	2.446
SC10	0.642	6.095	0.083	0.830	2	20	2.446
SC11	0.642	6.945	0.083	0.830	2	20	2.446
SC12	0.621	7.795	0.042	0.830	1	20	1.223
SC13	0.621	8.645	0.042	0.830	1	20	1.223
SC14	0.621	9.495	0.042	0.830	1	20	1.223
SC15	0.642	10.138	0.083	0.415	2	10	1.223
SC16	0.621	11.033	0.042	0.415	1	10	0.612
SC17	0.621	11.675	0.042	0.830	1	20	1.223
SC18	0.621	12.525	0.042	0.830	1	20	1.223
SC19	0.621	13.375	0.042	0.830	1	20	1.223
SC20	0.621	14.225	0.042	0.830	1	20	1.223
SC21	0.621	15.075	0.042	0.830	1	20	1.223
SC22	0.621	15.925	0.042	0.830	1	20	1.223
SC23	0.621	16.775	0.042	0.830	1	20	1.223

Table 6.1.1: Reference geometry and winding configuration for the solenoids of the target, decay and capture channel, also reporting the operating current for each solenoid module.

The design developed has progressed significantly in terms of magnet engineering, and we have reached the stage of initial engineering details on:

- conductor design and performance, including cooling, operating margin, quench detection and protection analysis [ref] ===> *should this be the bibitem for the VIPER cable ([329]) ?, cited in the figures];
- mechanical analysis, down to the level of the HTS tapes in the conductor [328];
- coil manufacturing, including winding technology, joints and terminations, and impregnation;
- mechanical structures, supports and screens, cryostat and integration with thermal screen and target.

A double pancake winding using a force-flow cooled HTS superconductor seems to be a good solution, meeting most design criteria. The force-flow conductor proposed for the study is largely inspired by the VIPER developed for magnetically confined fusion, and has already an experimental basis of proven performance [12]. The conductor is made by a hollow copper core hosting soldered stacks of REBCO tape. This cable is then enclosed in a steel jacket that only has structural functions. Most interesting, it seems indeed possible to achieve high field, 20 T peak field on axis, at high operating temperature, 20 K, which has benefits of lower capital and operation expenditure (CAPEX and OPEX) compared to previous solutions.

Cooling at high temperature, 20 K, with gaseous helium is not a trivial extrapolation of force-flow supercritical helium near liquid conditions, 4.2 K. High operating pressure, e.g. 20 bar, and larger temperature increase than usual, e.g. 3 K, will be mandatory to avoid excessive distribution losses, and achieving the gain in cryogenic efficiency associated with the higher operating temperature. More studies, integrating the refrigeration cycle, will be necessary to produce an optimal system.

Some additional features have been identified, that could make construction and operation simple. One such example is the reinforcement jacket which has no leak tightness requirement. The studies reported here also show that thermal stability will not be an issue. At the same time quench detection and protection can likely rely on well-established precise voltage measurement, reasonable detection threshold, in the range of 100 mV, and dump voltages within state-of-the-art technology, 5 kV. The hot spot temperature remains well below 200 K in all cases analyzed. It will be very interesting at this point to realize and test samples of the conductor designed here, to confirm manufacturing features, validate the performance reach and margins, and characterize the behavior during quench.

On the side of mechanical design, the overall criteria at the coil level can be satisfied within the allowable limits of common material grades. However, looking at the details of the stress and strain distribution within the cable we may have identified locations and conditions where loads could exceed allowable limits. Tensile and shear stresses at the level of the single tapes could reach values in the range of 60 MPa, whereby it is well known that the internal structure of REBCO tapes is not very resilient to this type of loading, with a wide spread of maximum allowable in the range of a few MPa and up to few tens of MPa. Note that while the analysis was performed for the specific geometry considered here, this may be a result of general applicability to soldered and twisted stacks of tapes. The analysis on this topic is only at the beginning, some avenues have been suggested to resolve this issue, and more optimization work is required, also considering the on-going work in the R&D program being pursued for fusion reactors [20]. Also in this case, some strong experimental evidence will be necessary to advance understanding and validate the solutions found.

The level of detail reached can be appreciated by sample views of the conductor, winding and 3D coil model shown in Figs. M2 and M3. While management of weights and forces remains challenging, we could find valid engineering and integration solutions for all above aspects, and we can be reasonably confident to proceed further with this baseline.

Work is in progress at present to advance in the engineering design of the chicane magnets, whose configuration and geometry has only been sketched. Achieving the required magnetic field profile in the large bore required will be a particular challenge because the radiation load from the spent proton beam is very high, possibly limiting the technology to resistive electromagnets.

In parallel, we are evaluating the implications of an increase of the beam power on the target, up to 4 MW which would allow to double the number of muons generated. While this will require additional shielding, and thus an increase of the bore dimension, first evaluations seem to indicate that it would still be possible to accommodate such an increase in performance with the present concept.

Fig. 6.1.2: Schematic view of the conductor configurations selected for the solenoid coils of the target, decay and capture channel (left) [329], with an image of a mock-up produced on real size (right) showing the HTS tapes, central copper former and jacket.

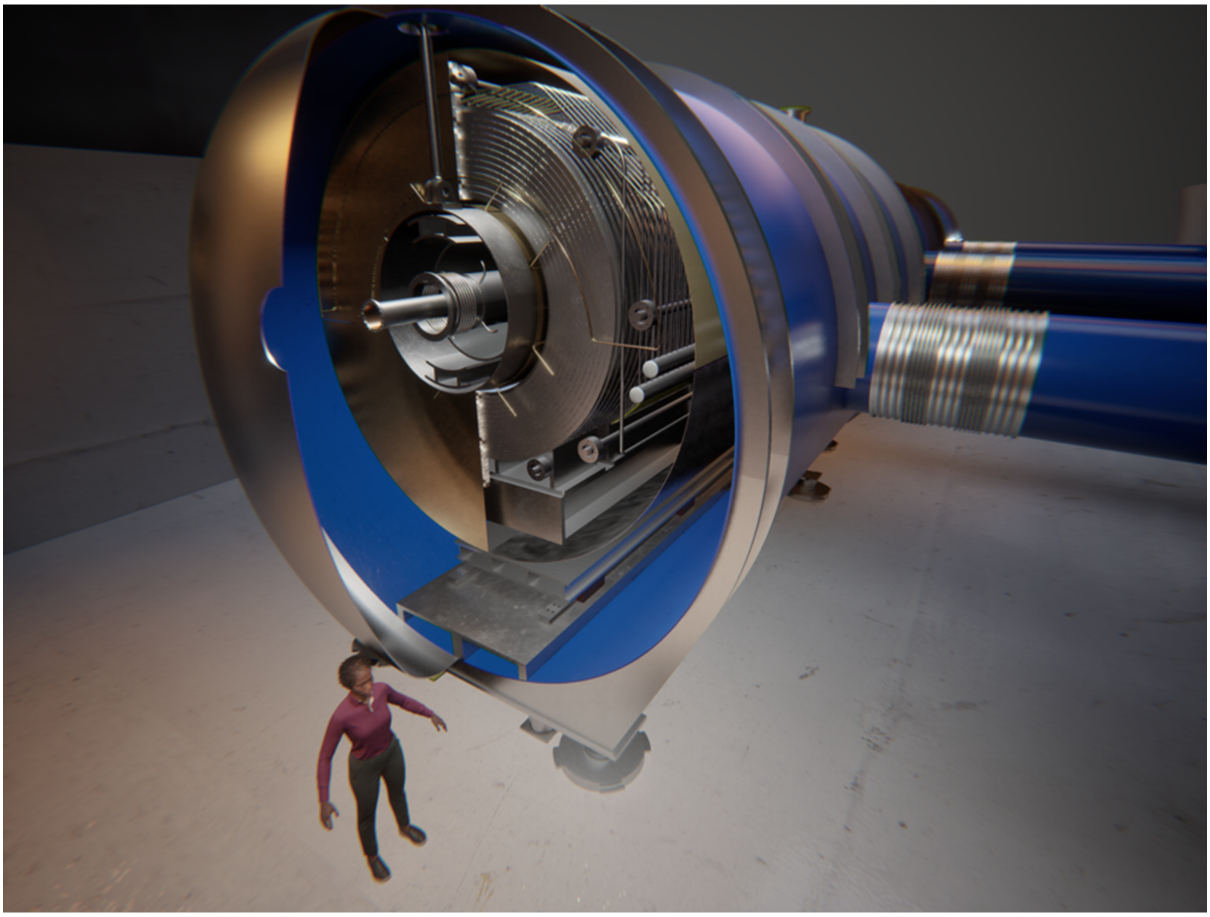

Fig. 6.1.3: Rendering of the magnet system for the target, decay and capture channel integrated in the cryostat, showing details of the winding, joints, cooling channels, thermal screen and supports.

6.1.0.1 Challenges Identified

As a result of the studies performed, we could identify a number challenges, to be addressed in priority:

- High-current HTS conductors qualified for operation in high field and helium gas. Although this class of conductors is being developed for fusion applications, the geometry selected needs experimental validation, especially to address the concerns of internal strain and stresses;
- Winding technology. The specific solution envisaged is well established, based on double pancakes wound from an insulated conductor, wrapped with fiber glass, stacked and vacuum impregnated with resin to form a coil module. Still, this was never applied to a HTS coil of this size, and this field level. Furthermore, novel solutions need to be developed for the soldering of the tape stacks in the cable, performed after winding, joints and terminations, as well as diagnostics for operation and protection;
- Radiation hardness of magnet materials, foremost polymers (insulation) and superconductor (REBCO). According to the expected radiation loads in a muon collider, both material classes will be at the expected limit of degradation. In addition, for HTS we lack a well-established material database and physical understanding of degradation mechanism.

6.1.0.2 Target Solenoid Model Coil

A magnet system of this field and dimension is a very challenging realization, depending on the success of a new technology, HTS, which is not yet deployed on large scale. This is why, as part of the next study phase, we propose to design, build and test a Target Solenoid Model Coil (TSMC) that shall demonstrate HTS force-flow cooled magnet technology at relevant scale, addressing two of the challenges listed above. The optimal TSMC configuration is presently under study, balancing performance in relevant conditions vs. affordable cost. A suitable configuration for the TSMC is shown in Fig. M4, a solenoid with a 1 m inner bore diameter, 2.3 m outer diameter and 1.4 m height. Preliminary targets chosen to map closely the operation of the coils of the target, decay and capture channel, are:

- Bore field of 20 T at 20 K operating temperature;
- Electromagnetic pressure J B R in excess of 500 MPa;
- Stored energy in excess of 100 MJ;
- Operating voltage of 2.5 kV;

Achieving above on a magnet of this size will give sufficient confidence in the realization of the full magnet system. The details of the proposal, including timeline, milestones, deliverables and resources, are detailed later, as well as in the companion paper [ref].

6D cooling channel solenoids

The 6D "beam cooling" process occurs over a 1 km long sequence of tightly integrated absorbers, alternating polarity solenoids, and RF cavities. The US-MAP design study provided a baseline configuration of a 6D cooling channel, consisting of 826 cooling cells over an approximate 970 m distance, with a total of almost 3000 solenoids [300]. These cells can be divided into 12 unique types termed A1-A4 and

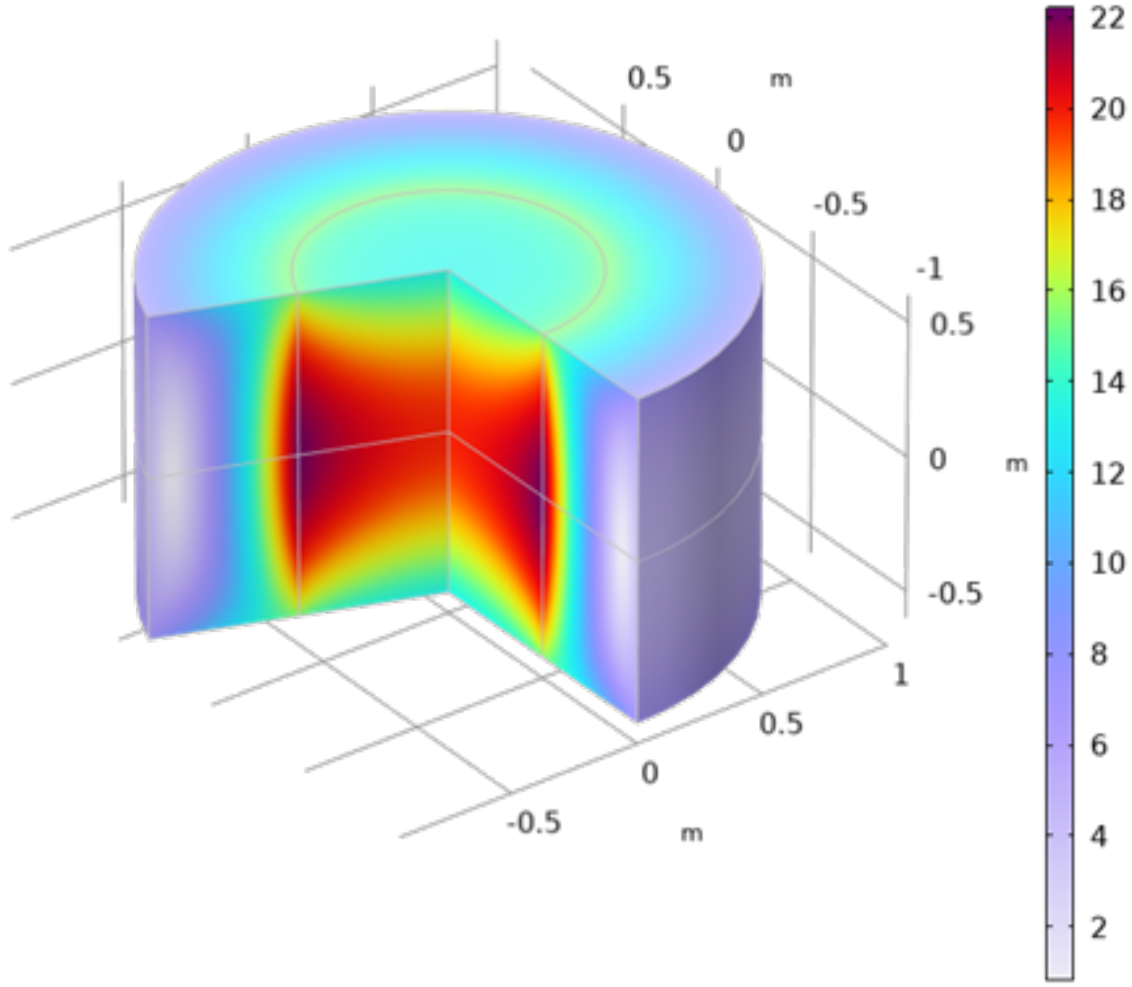

Fig. 6.1.4: A first result of configuration optimization for the design of a Target Solenoid Model Coil (TSMC) and corresponding field map in nominal operating conditions.

B1-B8 and ranging in length of ** to **. Each cell type contains between 2 to 6 solenoids, with a total of 18 unique solenoid types. For example, cell A1 has 4 solenoids, all of the same type, labeled A1-1, while cell B8 has 6 solenoids, of three different types, labeled B8-1, B8-2, and B8-3. The solenoids exhibit a diverse range of parameters, from small-bore to large-bore (90 mm to 1.5 m) and modest field to high field on-axis (2.6 T to 13.6 T). Each cell repeats a certain number of times (Ex. cell A1 repeats 66 times), before progressing to the next cell type. Fig. **??** displays the on-axis field of each cell type (assuming it is nested in a lattice of cells), and the solenoid cross-sections.

We performed an analysis on these solenoids, considering them operating individually and within their respective lattice. The results are reported in Table 6.1.2. We found substantial stresses (large hoop and tensile radial stress), forces (37 MN axial force), and quench management challenges (energy densities up to 91 MJ/m^3 in a single coil).

Such values suggest that the solenoid configuration may need further optimization to reach engineering level. This is a non-trivial task, because the beam optics in the solenoids of the muon cooling channel is far from being formalized as well as that of a collider, and any change in magnet engineering may have dramatic effects on beam transmission. Recognizing this challenge, we have developed

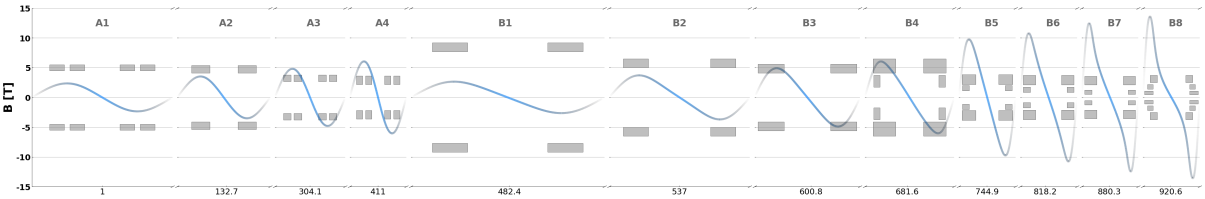

Fig. 6.1.5: Condensed schematic of the 12 types of cooling cells (A1 to B8) of a muon collider from the MAP configuration [300], with solenoid cross sections and the on-axis B_z field assuming each cell is in a lattice of neighboring cells of the same type. z-axis values shown correspond to the the middle of the first cell of each type.

Cell	E_{Mag} (MJ)	e_{Mag} (MJ/m^3)	Coil	$\boldsymbol{J_E}$ (A/mm^2)	B_{peak} (T)	σ_{Hoop} (MPa)	σ_{Radial} (MPa)
A1	5.4	20.5	A1-1	63.25	4.1	34	-5/0
A2	15.3	75.8	A2-1	126.6	9.5	137	-28/0
A3	7.2	72.8	A3-1	165	9.4	138	-29/0
A4	8.4	91.5	A4-1	195	11.6	196	-49/0
B1	44.5	55.9	B1-1	69.8	6.9	95	-14/0
B2	24.1	61.8	B2-1	90	8.4	114	-20/0
B3	29.8	88.1	B3-1	123	11.2	173	-37/0
B4	24.1	42.4	B4-1	94	9.2	231	0/20
			B4-2	70.3	7.8	66	-24/0
B5	12	86.3	B5-1	157	13.9	336	0/21
			B5-2	168	12.3	159	-55/0
B6	8.2	68.3	B6-1	185	14.2	314	-1/22
			B6-2	155.1	10.3	118	-43/0
B7	5.6	58.6	B7-1	198	14.2	244	-1/21
			B7-2	155	10.1	118	-37/0
B8	1.4	20.3	B8-1	220	15.1	255	-3/22
			B8-2	135	6.2	110	-2/5
			B8-3	153	6.2	41	-23/0

Table 6.1.2: Table of various parameters for 12 cell types and 18 unique solenoid types in the MAP configuration. Values correspond to solenoids operating in their respective cells within a lattice. Note that if the solenoid is operating stand-alone or in a single cell, some parameters take on higher or lower values.

solenoid design rules that implement simple engineering limits on operating margin, stress and stored energy density. These rules are integrated already at the stage of the beam optics design, thus anticipating magnet performance limits. Having the design rules as part of the beam optics optimization has reduced the iteration time and improved effectiveness of each design optimization. In parallel, we have developed numerical optimization tools which can scan design variants and improve the solenoid configuration given a desired field profile. Such tools allow to converge to optimal engineering solutions once the initial solenoid configuration is close enough to being feasible. These two advances, the solenoid design rules and optimization tools, are described in the next sections.

6.1.0.3 Solenoid design rules and limits

Solenoid engineering design rules have been defined and are presently used by the IMCC to improve upon the configuration originated by US-MAP and constrain new evolving optics studies and further magnet optimization studies. The design rules are analytical or semi-analytical expressions that provide solenoid performance limits, based on material and engineering parameters such as the superconductor critical current density (J_c) and the required operating margin, the known superconductor behavior under mechanical stresses σ_r, σ_θ and σ_z and strain, the associated mechanical limits on structural materials, and magnet protection for given stored magnetic energy density (e_m). To assess solenoid performance limits we generally assume that the superconductor is HTS (ReBCO) using critical current and stress limits that can be obtained from state-of-the-art industrial production [**Fujikura**], [**fujita2019flux**]. The J_c dependence on the operating temperature T_{op} and the field B_{op} was based on values obtained from measurement in field perpendicular to the tape plane (in a solenoid this is B_r) [**bordini2024conceptual**], which is a conservative assumption.

For the analyses reported here, we have set an operating temperature at $T_{op} = 20$ K and request an operating margin of 2.5 K. The maximum average hoop stress (σ_θ) is limited to 300 MPa [**Fujikura**] [**weijers2010high**]. Although HTS has showed resilience at higher values, we take a considerable margin to account for 3D stress distribution and the potential of induced stresses during quench, from magnetization currents, and other engineering uncertainties. For the radial stress (σ_r), we consider a maximum compressive stress of 300 MPa and a maximum tensile stress of 20 MPa [**Fujikura**]. The maximum tolerated tensile σ_r before degradation of the superconductor is approximately 10-100 MPa [**maeda2013recent**]. To avoid any tensile σ_r, a coil can be wound in tension generating a compressive pre-stress, such that there is no tensile σ_r when energized [**song2017engineering**], making our initial tensile σ_r limit possibly conservative. Although we have no analytic description of the stress parallel to the axis of the solenoid (σ_z), we note that a compressive σ_z can be tolerated up to 100 MPa [**Fujikura**].

Lastly, the energy stored in these superconducting solenoids will be very large, and in the event of a quench (loss of superconductivity in the conductor), this energy will dissipate into heat. To prevent damage to the magnet during a quench from excessive temperature rise and induced stresses from non-uniform material expansion, managing this stored magnetic energy is crucial. At this preliminary stage, a simplified estimation of the temperature rise during a quench can be computed assuming the magnetic energy is deposited homogeneously in the solkenoid. For a magnetic energy density in the range of 150 MJ/m^3 (corresponding to about 17 kJ/kg), the temperature rise of a HTS tape would be about 130 K. Although we are aware that much more effort is required for quench modeling, such temperature rise is modest, and we take this range of energy density as an initial acceptable upper limit. Future detailed quench analysis studies will be necessary.

The engineering limits are summarized in Table **. They provide an initial framework for iterating the design study of all 6D cooling solenoids, while in parallel more detailed engineering analysis is being carried out for a proof-of-principle 6D cooling cell demonstrator with HTS solenoids. (QUESTION to Siara: these are actually the design equations ? I would report them there, not just the limits)

A useful visualization tool of the key design parameters and their corresponding imposed limits described above is a plot of magnet aperture (A) vs. magnetic field (B), which we dubbed (A-B)-plot, where B is the maximum possible field on-axis (B_0 in Eq. **??**). Such plots have been part of the

Parameter	Unit	Lower bound	Upper bound
σ_θ	MPa	0	300
σ_r	MPa	-300	20
e_m	MJ/m^3	-	150

Table 6.1.3: Limits on select single solenoid parameters.

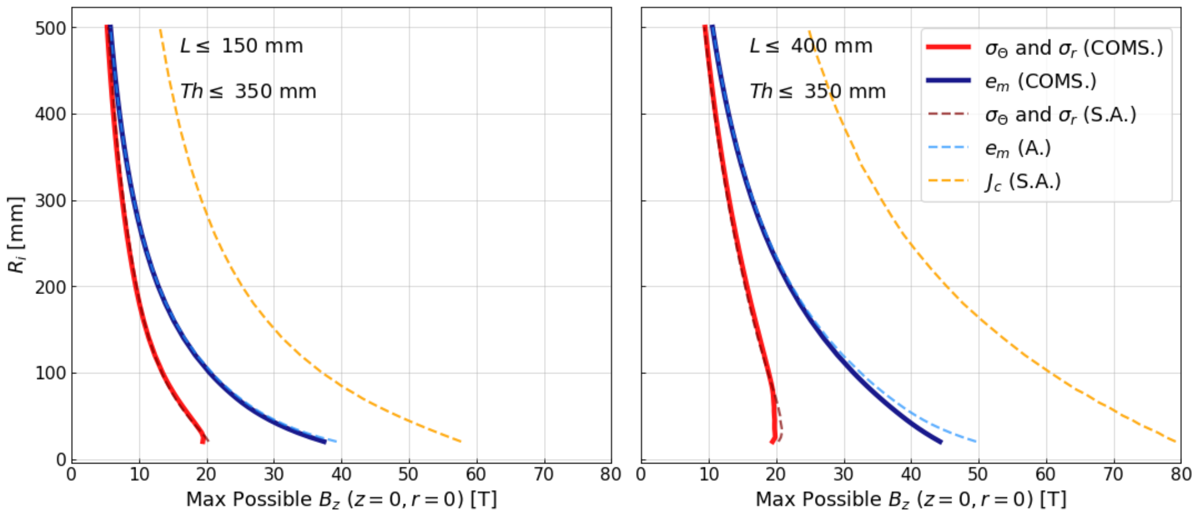

Fig. 6.1.6: The approximate maximum possible B_z on-axis versus bore radius (R_i) of a single solenoid with a maximum thickness of 340 mm and a length up to 150 mm (top) or 400 mm (bottom), for different limiting parameters: red curves correspond to stress limits, blue to the magnetic energy density limit, and orange to the critical current density. Solid lines correspond to results found numerically with COMSOL (COMS.), and dashed lines to analytic or semi-analytic Eqs.

conceptual design process for the dipoles of the collider [**novelli2024analytical**], and here we extend this concept to the solenoids of the 6D cooling. However, when considering solenoids there is added complexity because both the length and thickness of a solenoid can vary at a specified aperture. Figure 6.1.6 shows two example A-B plots for different limits of L, with limit curves of σ_r σ_θ obtained semi-analytically.

6.1.0.4 *Solenoid Optimization Tools*

The initial configuration resulting from the beam optics studies, although satisfies the design guidelines described above, is not necessarily an optimized engineering solution. To improve the magnet configuration, we have created a numerical code, partly written in-house and partly based on proprietary software (COMSOL), termed the Solenoid in-Cell Optimization program (SiCO). This program is built to optimize solenoids that produce a desired field profile and tolerance. It can be broken down into three steps, characterized by set-up, computation, and filtering based on the desired field profile and design rules. With this tool millions of solutions can be computed very quickly, allowing the choice of the best solenoids depending on weighted design criteria such as stress, stored energy, or coil volume (and associated cost). In addition, the code can cope with considerations of standardization (choosing solenoids with identical geometry across cells), or powering and quench protection.

We used this code to analyze cells A1 to B3 of MAP, considering 2 coils per cell. Analysis of cells with coils at multiple radii (B4-B8) is ongoing and will be presented in the future. Figure **??** presents the minimum achievable volume of conductor per cell for A1-B3, and the corresponding cell e_m and single coil stress σ_θ (values computed with COMSOL for solenoids in a lattice).

FIGURE – RESULTS FOR MAP

To achieve the minimum volume while maintaining the field profile, the current densities increase to values ranging from 160 A/mm^2 (B1-1) to 402 A/mm^2 (A3-1). As expected, the hoop stresses and stored magnetic energies also increase (see Tab. **??** for comparison). However, other parameters stay similar or improve. The compressive radial stresses are low (maximum of 35.4 MPa in coil A4-1, compared to 49 MPa in MAP), with no tensile radial stress. The peak fields in the conductor are similar, with a maximum fraction of J_c reached in A3-1, with $J = 0.57J_c$ ($B_{\text{peak}} = 8.2$ T). The net longitudinal forces are significantly smaller across all the solenoids ($F_z = 36.8$ MN in MAP compared to $F_z = 12.4$ MN here for B3-1).

This solution set demonstrates the success of the power of this numerical optimization tool to search for solenoid configurations depending on weighted design criteria and technology options. It provides an excellent starting point for more detailed mechanical analysis, where parameter limits can be easily changed to generate new solution spaces depending on evolving understandings. The overall workflow is summarized in Fig. ***.

6.1.0.5 First evaluation of present baseline cooling optics from IMCC

We have applied the above procedure to the new optics developed recently for the 6D cooling channel. The new otpics achieves an output transverse emittance that is half of what was achieved in previous studies [301]. This will aid in reaching a lower overall final emittance before acceleration and collision, a substantial gain of performance for the collider. During these beam dynamics studies, solenoid geometries and their corresponding field maps (among other parameters) are iterated on. To constrain the allowable magnet geometries and current densities, the 'design rules' described above were directly integrated into the beam optics optimization routine. This yielded a final optics with assumed solenoid geometries within or near allowed design limits, summarized in Table ***.

This latest initial optics configuration has a total of 3030 solenoids in one 6D cooling chain, with a peak field on-axis broadly increasing from 2.6 T to 17.9 T. There are 26 unique solenoid types, with bore radii ranging from 25 mm to 400 mm, lengths from 75 mm to 287 mm, and current densities from 58 A/mm2 to 327 A/mm2. As seen in Table **, the solenoids experience substantial peak fields at the conductor (up to 19 T), large stresses and forces. However these values are not far off target limits, and can be optimized further. The initial solenoid configurations also exhibit tight spacing, and needs to better factor in room for RF structure and waveguides. These additional parameters (magnet spacing, RF required spacing), will be factored into the next iteration of the beam optics optimization.

This is presently work in progress, but demonstrates already that the preparatory work is paying back with beam optics solutions closer to engineering feasibility. Our plan is to proceed towards an updated configuration, taking into account spacing requirements, and apply the SiCO numerical optimization to search for more ideal solenoids given desired field profiles.

Solenoid design applied to the RFMFTF and demonstrator (watch for overlaps with demonstra-

Cell	E_{Mag} (MJ)	e_{Mag} (MJ/m^3)	Coil	$\boldsymbol{J_E}$ (A/mm^2)	B_{peak} (T)	σ_{Hoop} (MPa)	σ_{Radial} (MPa)
A1	5.4	21	A1-1	57.6	5.2	42	-8/0
A2	22.1	106.1	A2-1	149.5	11.6	194	-48/0
A3	5.0	49.5	A3-1	131.5	10.1	121	-25/0
A4	8.0	92.3	A4-1	193.2	13.8	225	-51/1
B1	9.1	49.8	B1-1	96.9	7.7	104	-24/0
B2	15.6	64.2	B2-1	102.1	9.2	131	-32/0
B3	36.9	105.9	B3-1	127.9	12.9	208	-57/0
B4	75.6	149.9	B4-1	88.5	16.1	260	-1/29
B5	17.3	88.9	B5-1	179.6	14.7	295	-2/17
B5			B5-2	154.0	14.7	212	-57/1
B6	8.3	96.6	B6-1	214.4	15.3	339	-5/18
B6			B6-2	211.5	12.0	214	-6/6
B6			B6-3	212.7	12.4	162	-46/0
B7	8.2	87.7	B7-1	183.3	14.7	264	0/25
B7			B7-2	153.9	11.1	175	-4/10
B7			B7-3	210.3	13.2	180	-45/1
B8	8.8	92.1	B8-1	193.7	16.5	270	-6/38
B8			B8-2	202.1	15.4	270	-6/29
B8			B8-3	212.8	13.2	187	-50/0
B9	7.5	76.5	B9-1	256.4	17.2	281	0/37
B9			B9-2	88.4	10.0	95	-2/12
B9			B9-3	204.9	13.2	184	-46/0
B10	5.0	68.6	B10-1	326.8	19.2	378	0/49
B10			B10-2	146.1	11.1	105	-4/13
B10			B10-3	207.8	12.5	158	-43/1

Table 6.1.4: Table of various parameters for the 14 cell types and 26 unique solenoid types in the latest 6D cooling optics [301]. Hoop stress values reported correspond to the maximum, while radial stress values reported are the minimum/maximum. All values correspond to solenoids operating in their respective cells within a lattice. Note that if the solenoid is operating stand-alone or in a single cell, some parameters take on higher or lower values.

tor activities). Identified as crucial technology demonstrators are the RFMFTF and 6D cooling cell demonstrator (clarify these better*). The 6D cooling cell demonstrator will address a slew of magnet engineering difficulties seen across the various types of cooling cells, including large forces, stresses, stored energies and fields at the conductor. To be completed. . .

6.1.0.6 Challenges identified

The studies have highlighted two major challenges to be addressed in priority:

– Compact solenoid windings, achieving performance at minimum cost. The field reach of the single solenoids of the 6D cooling channel is not extraordinary. Indeed solenoids of this class have already been built. But the number of solenoids required is large. High current density, hence minimal use of superconducting material, is a key to making the 6D cooling practical and affordable. This implies mastering large forces and quench in compact windings, which needs demonstration. Note that high current density is also a key to reaching the required field gradients, see also below;

– Integration. A unique feature of the solenoids in the cooling cell is the need to generate an alternating field profile with high gradient, and host RF cavities and absorbers. This imposes opposing constraints on distancing and spacing, including the management of large electromagnetic forces among solenoids of opposite polarity, access requirements, and effective thermal management in tight space. Also this challenge requires practical demonstration;

Final cooling solenoids

Among the solenoids in the cooling channel, the final cooling solenoids are most challenging in terms of field performance, with a target of 40 T or higher. The bore dimension is relatively small, 50 mm, which makes them an ideal development vehicle to implement new technology such as non-insulated windings, and probe performance limits. Indeed, this solenoid is an ideal vehicle for R&D, allowing fast turn-around models and tests that are relevant to magnets of larger dimension, such as the solenoids for the 6D cooling. This is why we have advanced very swiftly in the conceptual and engineering design of the 40 T final cooling solenoid.

We have proposed a conceptual design at the early stage of the study [330]. The solenoid concept is based on soldered single pancakes, stacked with stress-management plates, and joined electrically. The coil is pre-compressed radially by a solid mechanical structure, supporting the electro-magnetic loads, and necessary to avoid tensile stress in the coil at nominal operating conditions.

6.1.0.7 Concept and Engineering Design

The concept for the final cooling solenoid is shown schematically in Fig. M2, and it was developed at the outset of the study profiting from experience in other fields of science and societal applications. In the past twelve months we have focused on the development of engineering solutions for the realization [2]. Fig. M2 shows 46 identical modular pancakes and three pairs of thicker single pancakes at both ends of the solenoid. In Fig. M2, the arrows indicate the axial and radial Lorentz forces acting on each pancake, with their lengths proportional to the magnitude of the respective forces. To enhance readability, the lengths of the radial arrows have been scaled down by a factor of 3 relative to the axial arrows. Despite this difference in arrow lengths, the radial forces are nearly equal to the axial force on the outermost pancake, which is around 300 tons.

Moving radially outward from the solenoid axis and ignoring the two axial extremities, the components are as follows:

1. Internal Electrical Connection: This is a superconductor carrying an axial current, represented by yellow lines in Fig. M2, which connects two adjacent pancakes in series.
2. Internal Joint Ring: A 0.5 mm thick normal conducting ring that is electrically connected to the Pancake Coil and the Internal Electrical Connection.
3. Pancake Coil: This coil consists of ReBCO tape wound around the Internal Joint Ring, with adjacent turns soldered together to form a continuous solid block. For the Modular Pancakes, the coil features an inner radius of 30 mm and an outer radius of 90 mm, while the End Pancakes have a larger outer radius.

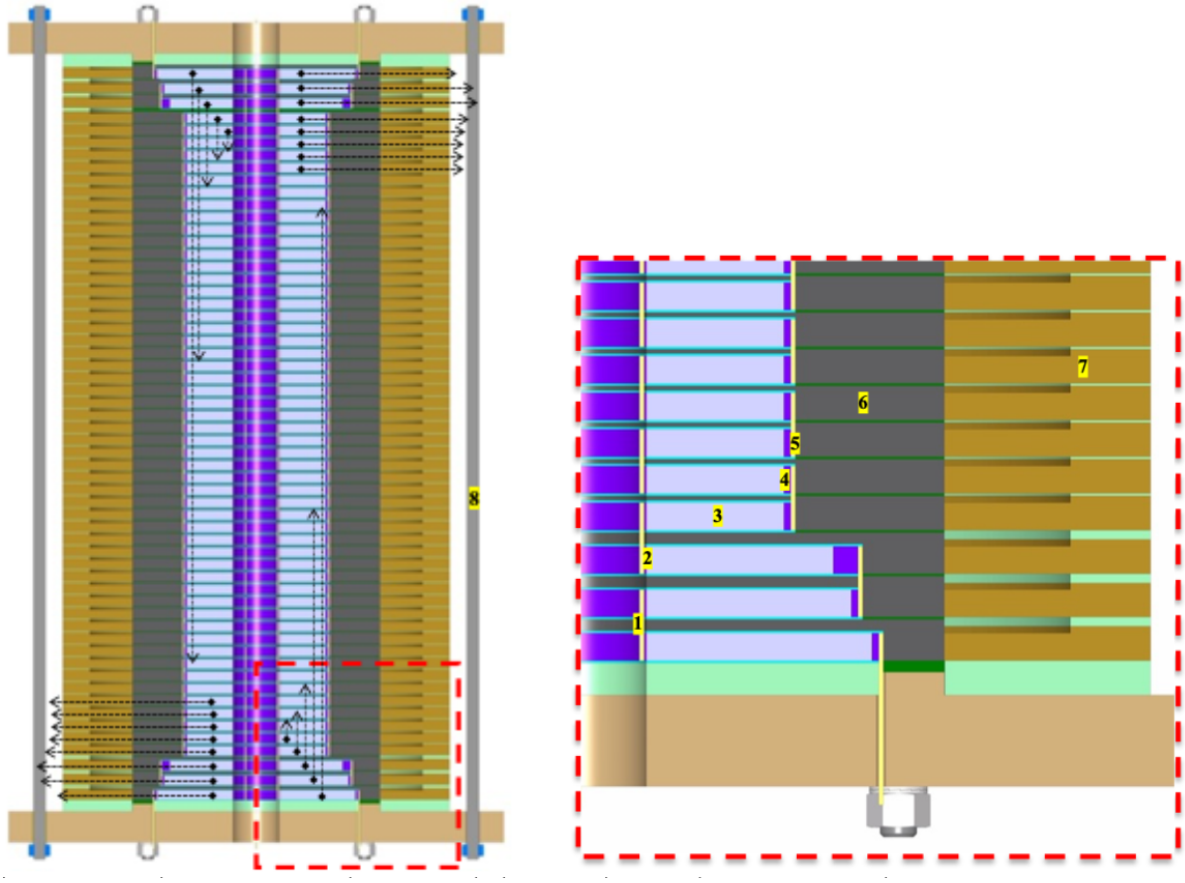

Fig. 6.1.7: Cross-section of the 40 T solenoid; the arrows indicate the axial and radial Lorentz forces acting on each pancake. The lengths of the radial arrows have been scaled down by a factor of 3.

4. External Joint Ring: A 5-mm-thick normal conducting ring electrically connected to the Pancake Coil and the External Electrical Connection.
5. External Electrical Connection: A superconductor carrying an axial current, represented by yellow lines in Fig. M2, which connects two adjacent pancakes in series or links the solenoid extremities to the current leads.
6. Support Cup: A single stainless steel (SS) piece, shown in dark grey, consisting of a 12 mm high disk and a 2 mm thick radial plate that separates two adjacent Pancake Coils. The Support Cups serve a dual purpose: (1) providing radial stiffness and pre-compression to counteract the radial expansion of the coils caused by Lorentz forces, and (2) intercepting axial Lorentz forces [1]. The pre-compression on each pancake coil is achieved through shrink fitting at room temperature after heating the Support Cup to approximately 100-200°C.
7. Pre-Compression Disk : A SS (or another structural material) disk, depicted in light brown, with a height of 12 mm in the central part and approximately 14 mm at the periphery. The Pre-Compression Disk delivers most of the radial pre-compression through shrink fitting at room temperature. In this scenario, the Pre-Compression Disk, located relatively far from the Pancake Coil, would be heated to temperatures above 200°C.
8. Axial Rods: Stainless steel bars that ensure good contact between adjacent Support Cups through the two flanges at the magnet's axial extremities.

Mechanical calculations [331] indicate that, when neglecting the contribution of magnetization and assuming sufficiently stiff radial plates, this design can maintain stress and strain within safe limits for the superconductor during regular operating conditions (excluding quenches). Table 6.1.5 provides an example of the calculated mechanical loads on the conductor at various stages: Room Temperature (RT), Step 1; at 4.2 K with no current in the conductor, Step 2; and at 4.2 K with the magnet energized to 40 T, Step 3. The table specifically refers to a case with a RT pre-compression of 200 MPa and an Internal Joint Ring thickness of 0.5 mm. These findings, along with other case studies, are discussed in detail in [3].

	Step 1	Step 2	Step 3
Radial Stress [MPa]: Min/Max	-205/-8	-190/-5	-290/10
Hoop Strain [%]: Min/Max	-0.25/-0.10	-0.20/-0.12	-0.04/0.28*

Table 6.1.5: Radial Stress and hoop Strain values across steps.

6.1.0.8 Quench Protection

The proposed design achieves a relatively low energy per unit length of approximately 5.4 MJ/m, thanks to the extreme compactness of the coil [1]. However, the magnetic energy per unit volume, or magnetic energy density, is relatively high at 300 J/cm³. If this energy were uniformly dissipated within the winding, the temperature would rise from 4.2 K to around 200 K. While 200 K is not considered a threat to the coil, the localized dissipation of this energy during a quench could irreversibly damage the magnet.

In traditional insulated, unprotected, low-temperature superconducting (LTS) coils, a localized quench typically results in conductor melting. To prevent this, detection systems are used to monitor resistive voltages and initiate a fast discharge, redirecting the energy to an external resistor via high voltage. An alternative strategy involves triggering a uniform quench across the entire coil, typically using resistive heating. In LTS accelerator magnets, this is achieved with internal heaters or current/field oscillations.

However, high-temperature superconducting (HTS) coils present unique challenges. Their substantial enthalpy margin and low quench propagation speed make quench detection using voltage measurements difficult. Furthermore, using quench heaters to uniformly quench the entire coil is impractical.

These challenges make it well known that insulated HTS coils with high magnetic energy density are very difficult to protect effectively against localized quenches. Consequently, the choice of non/metal-insulated (N/M-I) coils for the proposed conceptual design was strongly influenced by these considerations.

These coils have low thermal and electrical resistance between turns, enabling rapid quench propagation and reducing localized energy dissipation. N/M-I coils could also allow quench detection based on fast magnetic flux variations resulting from a quench due to the sudden increase/decrease of radial and azimuthal currents in the quenched region. Upon quench detection, the entire solenoid could be quenched by injecting a pulsed current between its terminals, with the current mainly flowing radially, leading to uniform rapid heating of the entire solenoid. The primary advantage of this quench strategy is achieving a symmetric and controlled quench, where the generated mechanical forces are known and reproducible [1].

Various protection strategies are currently under investigation [332, 333]. We recently investigated the potential of a capacitor discharge (CD) method for magnet protection, which, upon quench detection, injects a large current pulse into the full stack or individual pancakes, generating heat through the coil's turn-to-turn resistance. Most of this current flows through the low-inductance, radial turn-to-turn paths between the terminals of each pancake coil. The energy from the current pulse is dissipated as heat within the pancakes, using the turn-to-turn resistances as internal quench heaters. This approach rapidly raises the conductor temperatures above the critical temperature within milliseconds and requires no additional internal components, as it can use the magnet's existing current leads [4,5].

6.1.0.9 Magnetization and current distribution

To assess the impact of persistent currents on the mechanical loads acting on the Pancake Coils, a 2D thermal-electromechanical model was developed using COMSOL Multiphysics. The electromagnetic analysis was performed using a T-A formulation [4], and the resulting Lorentz forces were then applied as input to a thermo-mechanical model that simulates all 750 turns of the Modular Pancake, with a level of detail similar to the 2D model presented in [3]. For the electromagnetic model, it was assumed that adjacent turns of the winding are electrically insulated, which, although not entirely accurate, is considered conservative as it tends to yield higher mechanical load values.

The model shows that, due to persistent currents, the Modular Pancake closest to the End Pancakes experiences a 30% increase in the maximum strain on the conductor. This increase significantly diminishes in the subsequent pancakes, with the sixth Modular Pancake from the End Pancakes showing an increase of no more than 1%. The End Pancakes, however, exhibit an increase in maximum strain on the conductor well above 30%. Regarding the axial Lorentz forces, magnetization tends to reduce the axial Lorentz forces by straightening the magnetic field lines (Magnetization currents generate a radial field that opposes the radial field produced by the transport current.). For example, the aforementioned calculations show that the axial Lorentz forces acting on the outermost pancake are reduced from approximately 300 tons to around 260 tons. To mitigate conductor magnetization and the associated hoop strain we are exploring the use of striated tapes or the End Pancakes and for a few adjacent Modular Pancakes.

Progress has also been made in assessing the impact of quenches on the mechanical loads of the conductor. For this purpose, a 2D axisymmetric electrical and thermal network model developed in Python was coupled with a simplified 2D mechanical model in Comsol. Preliminary results indicate that in some quench scenarios, the maximum hoop strain could increase by up to 30% [4].

Currently, as noted in [334], there is no 3D model capable of accurately describing the transient behavior of large non-insulated (NI) ReBCO superconducting coils during quench events. However, a thorough understanding of these transient phenomena is essential to fully exploit the potential of this technology. While 3D Finite Element Method (FEM) models are the most promising approach for accurately capturing the magneto-thermal dynamics of these magnets, the widely used H formulation of Maxwell's equations for superconductors [335] remains computationally too intensive for simulating large-scale systems like accelerator magnets. To the authors' knowledge, 3D models based on the H-formulation are currently limited to very short lengths of superconducting tapes (a few meters) and even

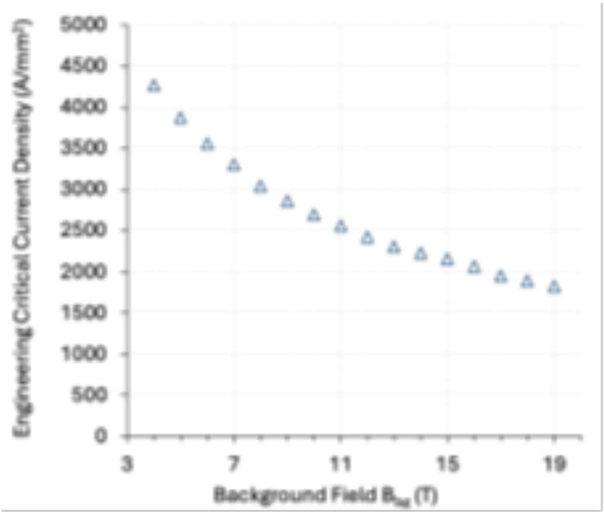

Fig. 6.1.8: Critical current measurements (triangles) at 4.2 K of a procured ReBCO tape (B // c-axis).

shorter lengths in the case of multifilamentary wires.

To address this issue, a novel mathematical formulation has recently been developed at CERN and integrated into the commercial FEM software COMSOL. Initial results suggest that this new approach could significantly reduce the computational time required for large-scale 3D FEM transient simulations of superconductors, demonstrating its potential to streamline these complex analyses (2). The model has already produced significant results for the project, enabling the quantification of the time required to energize the magnet to its target field as a function of the contact resistance between adjacent turns.

In addition to the COMSOL model, we have developed a 3D model that uses the H formulation for the electromagnetic analysis coupled with a thermal model, utilizing the open-source FEM software GetDP. This model has already been successful in studying quench evolution in a 20-layer pancake [336], and ongoing studies aim to reduce the computational time required by this approach, potentially enabling the simulation of larger systems.

6.1.0.10 Experimental Studies

The engineering studies outlined above are complemented by an intense campaign of electrical, mechanical and thermal measurements, necessary to establish the thermo-physical and mechanical properties of single tapes and stacks of tapes.

We have procured over 10 km of 4-mm-wide tape from three different companies: Faraday Factory Japan, Fujikura, and Shanghai Superconductor Technology. The goal is to begin producing smaller coils in the initial phase of technological development to manage costs effectively. We have initiated the characterization of the superconducting properties of the procured tape through critical current measurements at 4.2 K in a background magnetic field, oriented perpendicular to the transport current direction and the wide face of the tape, with fields up to 19 T. These measurements were conducted at the University of Geneva. Fig. M3 shows the results of the first sample measured which are outstanding, with an engineering current density exceeding 2 kA/mm2 at 16 T. This exceeds the performance requirements for the 40 T final cooling solenoid, proving that from this point of view the technology is accessible.

Accurate knowledge of the elastic-plastic properties, fracture toughness, and thermal expansion

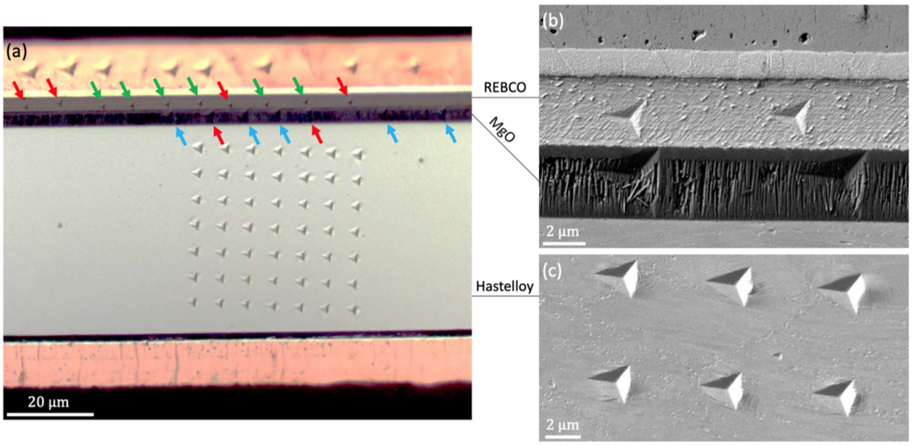

	Hastelloy	Copper	YBCO	MgO
	E (GPa)	E (GPa)	E (GPa)	E (GPa)
RD	197	84	155	95
TD	195	90	120	60

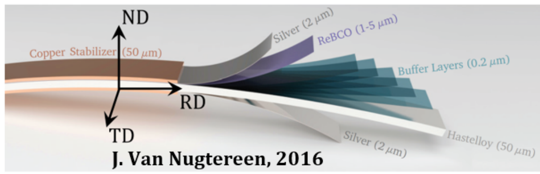

Fig. 6.1.9: (a) Optical image of the residual indentation imprints in the Hastelloy, copper, MgO (blue arrows) and REBCO (green arrows) layers. Red arrows indicate tests rejected due to being too close to other layers because of poor targeting. (b) SEM images of the residual indentation imprints in the REBCO and MgO layers. (c) SEM images of the residual indentation imprints in the Hastelloy layer. The measured values are summarized in the table.

of ReBCO materials is crucial for precise stress analysis in superconducting magnet systems. To address this, we initiated a comprehensive measurement campaign to determine the thermomechanical properties of ReBCO tapes and stacks. The campaign includes both macro and micro mechanical characterizations. The macro-scale samples consist of individual tapes or stacks a few centimeters long [ref, [337] correct?], while the micro-scale samples are micrometric pillars (micropillars) obtained through focused ion beam (FIB) milling of the individual layers of REBCO tapes [ref]. Additionally, nanoindentation measurements were performed [ref]. Although we are just at the beginning, this campaign has already yielded valuable results, including data on the thermal expansion properties of various REBCO tapes [ref], as well as insights into the elastic modulus, yield stress, plastic flow behavior, and fracture toughness of the different layers within the REBCO tapes [ref].

In parallel, we are starting the winding of single pancakes that match well the dimensions and properties of the final cooling solenoid design. These pancakes, tested singularly or stacked in small coils, will serve as the main R&D vehicle to develop and validate engineering solutions. We are exploring two approaches for soldering the coils: either after the winding is completed or during the winding process. For the latter, we have designed and manufactured a custom winding machine, which is currently being commissioned. Meanwhile, we have initiated a testing campaign to evaluate the quality of different soldering techniques on tape stacks and small pancakes. After soldering, the samples were analyzed using X-ray Computed Micro Tomography and micrographic techniques to assess the level of residual porosity. For the pancakes, critical current measurements were also performed. The results obtained so far are encouraging, demonstrating that it is possible to completely fill the gaps between the tapes when precompression is applied during soldering. Moreover, the critical current measurements

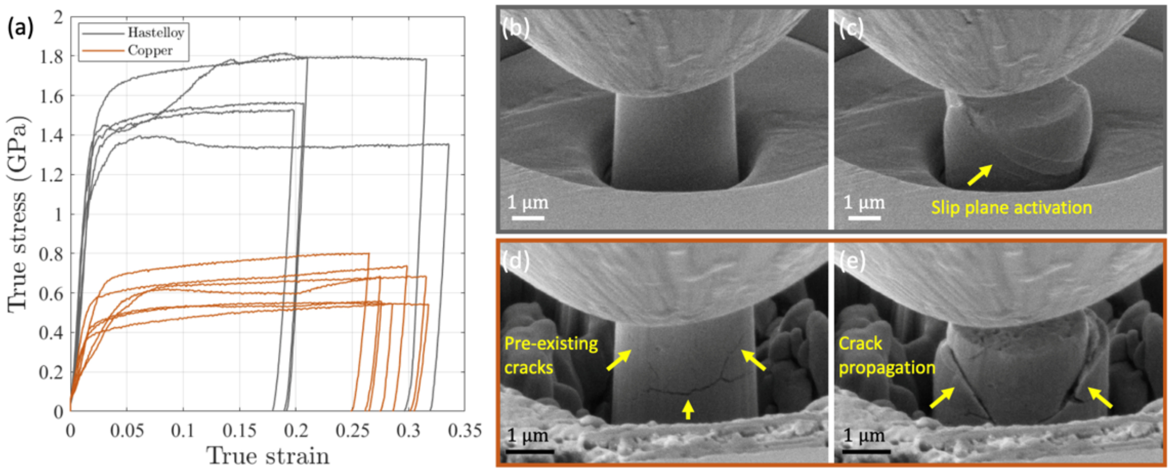

Hastelloy		Copper	
σ^y / GPa	* ε^y / %	σ^y / GPa	* ε^y / %
1.2 – 1.6	0.61 – 0.82	0.4 – 0.6	0.42 – 0.66

Fig. 6.1.10: (a) True stress-strain curves of Hastelloy and copper layers obtained by micropillar compression. (b)-(c) SEM images of a representative Hastelloy pillar before and after compression, respectively. (d)-(e) SEM images of a representative copper pillar before and after compression, respectively. The measured values are summarized in the table.

indicated that the tapes can be soldered without degrading their superconducting properties.

As a final remark on this aspect of the work performed, the methods developed and the data collected constitute a unique knowledge database which is useful also for other HTS magnets, relevant both to HEP as well as other fields of science and societal applications. This additional result, driven by the IMCC activities, deserves special recognition.

The plan in the coming months is to further increase experimental activities, especially the manufacturing and testing of pancakes and conducting critical current measurements at 4.2 K. Once the new winding machine is commissioned, we expect to produce a large number of pancakes in 2025. The inner radius of the superconducting winding is fixed at 30 mm, while for the outer winding diameter (OWD) different values will be tried.

1. We will start producing coils with OWD equal to 35 mm in order to minimize the use of conductor; the goal of these coils will be
   (a) Verify that we can solder together adjacent turns with a negligible porosity and without degrading the superconducting properties (tomography, microscopies, critical current measurements at 77 T);
   (b) Asses the transverse contact resistance associated with fully soldered coils when using the 3 conductors procured.
   (c) Study possible solution to modify the transversal contact resistance;

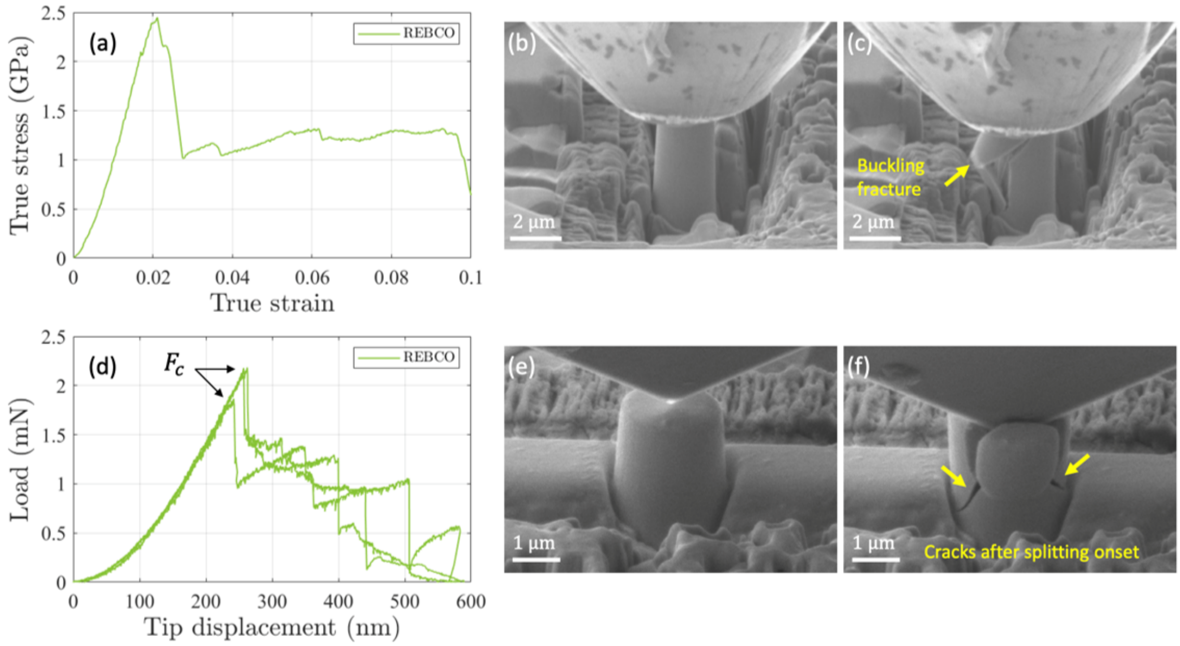

	REBCO		
	E (GPa)	σ_y (GPa)	K_c (MPa$\sqrt{\text{m}}$)
RD	155	4.00	1.34 ± 0.12
TD	120	2.80	0.56 ± 0.02

Fig. 6.1.11: (a) True stress-strain curve obtained by compression of a REBCO micropillar. (b)-(c) SEM images of the REBCO pillar before compression and after the first fracture, respectively. (d) Load-displacement curves obtained from splitting REBCO micropillars. (e)-(f) SEM images of a representative REBCO pillar before splitting and after the first fracture, respectively. The measured values are summarized in the table.

   (d) Study the electrical properties of different joints solutions

2. We will then increase the winding thickness to 50 mm OWD, so that piling up a few of these coils will allow to reach significant field in the centre of the solenoid (about 20 T at 4.2 K); main goals

   (a) Verify the feasibility of applying a radial precompression via shrink fitting without damaging the superconductor and the joints (tomography , critical current measurements at 77 K) of a single pancake

   (b) Verify that the coils do not degrade because of the Lorentz forces once energized at 4.2 K and with a current value that would allow to generate a field of 20 T when piling up several coils.

Further increase of winding thickness, and higher field levels, will depend on the result of the above phases.

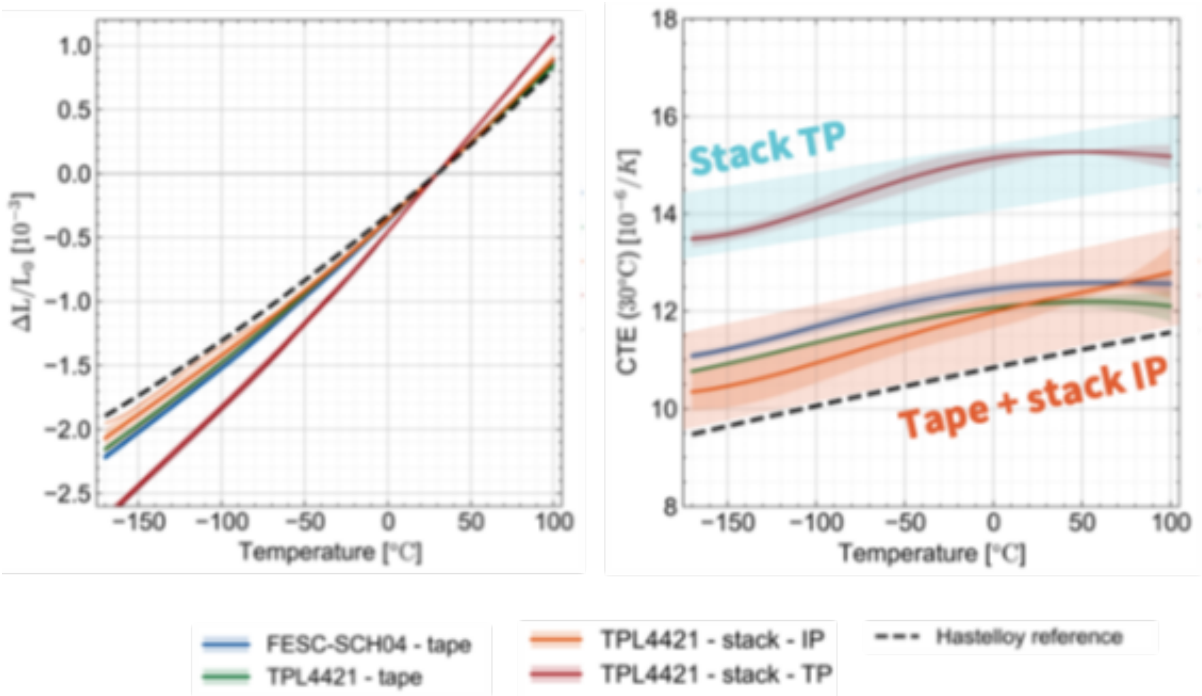

Fig. 6.1.12: Thermal contraction measurements of 2 ReBCO tapes (Theva TPL4421, and Fujikura FESC-SCH04) and of a soldered tape stack made with TPL4421. The measurements were carried out only along the In Plane (IP) direction for the tapes, while for the stack also the Through Plane (TP) measurements were performed

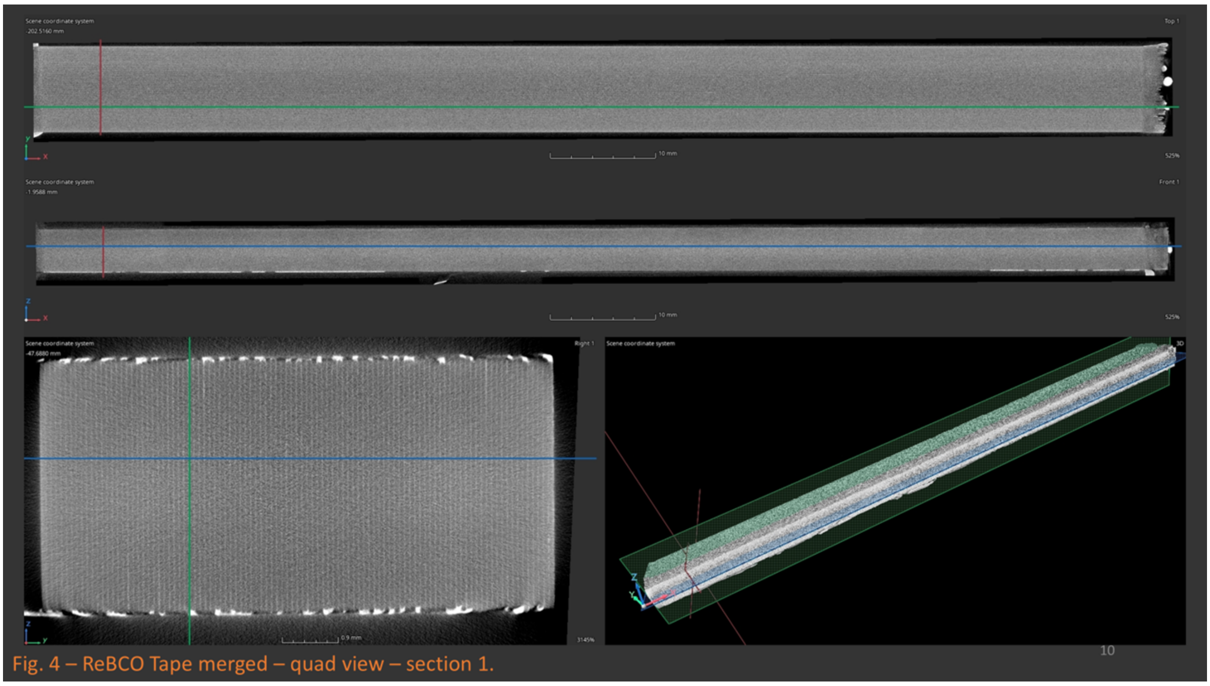

Fig. 6.1.13: Tomography of a stack of ReBCO tapes soldered under vacuum – negligible porosity achieved.

6.1.0.11 Challenges identified

Achieving a bore field of 40 T in the final cooling solenoid is a grand challenge, no such magnet exists today. Success will depend on mastering the following aspects:

- Mechanics. The design stress is at the expected material limit, and we are aware that ReBCO tapes can stand minimal shear stresses along the superconductor plane and minimal tensile stress in the direction perpendicular to the superconductor plane. The design shall demonstrate excellent control of the large variation of the strain/stress state on the conductor before and after energization, with no stress concentration;
- Quench protection. This will depend on the ability to control the transverse resistance, as well as early quench detection to trigger a power supply trip, so to discharge the energy in a controlled fashion, preventing excessive temperatures and mechanical stresses/strains. A controlled and reproducible electrical and thermal transverse ensuring is crucial for magnet protection, while allowing for reasonable magnet energization times;
- Novel magnet technology. Several features need to be demonstrated, like the ability to control winding geometry and a soldering between winding with a minimal amount of porosities, to control pre-compression via shrink fitting and/or alternative methods making sure to avoid coil buckling or degradation, and joints that can properly distribute the current in the coil while avoiding excessive heating and mechanical stresses.

Accelerator magnets

The largest number and most challenging magnets of the acceleration chain are those in the Rapid Cycled Synchrotrons (RCS) and Hybrid Ramped Synchrotrons (HCS). Among the several configurations studied, we have settled on common specifications for the dipole magnets of all stages, namely:

- Resistive dipoles with 1.8 T peak field and 30 mm (H) x 100 mm (W) rectangular aperture. These dipoles are pulsed with ms time scale at a frequency of 5 Hz. In the RCS they are ramped from injection to peak field (two quadrant), while in HCS they swing from negative to positive peak field (four quadrant);
- Superconducting dipoles with 10 T peak field and the same 30 mm (H) x 100 mm (W) rectangular aperture. These dipoles operate in steady state and provide the field offset for the HCS.

Both magnet types require field homogeneity in the range of few 10-4 in the good field region. Quadrupole magnets are still a subject of study, whereby we are scanning designs producing gradients in the range of 30 T/m in an aperture in the range of 40 mm to 80 mm, as discussed later.

The above magnet specifications require care and optimal design, and possibly better knowledge of magnetic and resistive properties of materials in the range of ramp-rates and frequencies required, but they appear well within the capabilities of present magnet technology. In fact, the main design driver for RCS and HCS is the management of the magnetic energy and reactive power, which should be highly efficient to minimize losses and very precise to meet beam performance specifications. To set orders of magnitude, the stored energy of a resistive magnet with the above characteristics is of the order of 6 kJ/m. The RCS have lengths in the range of 7 km to 27 km, and the total stored magnetic energy will

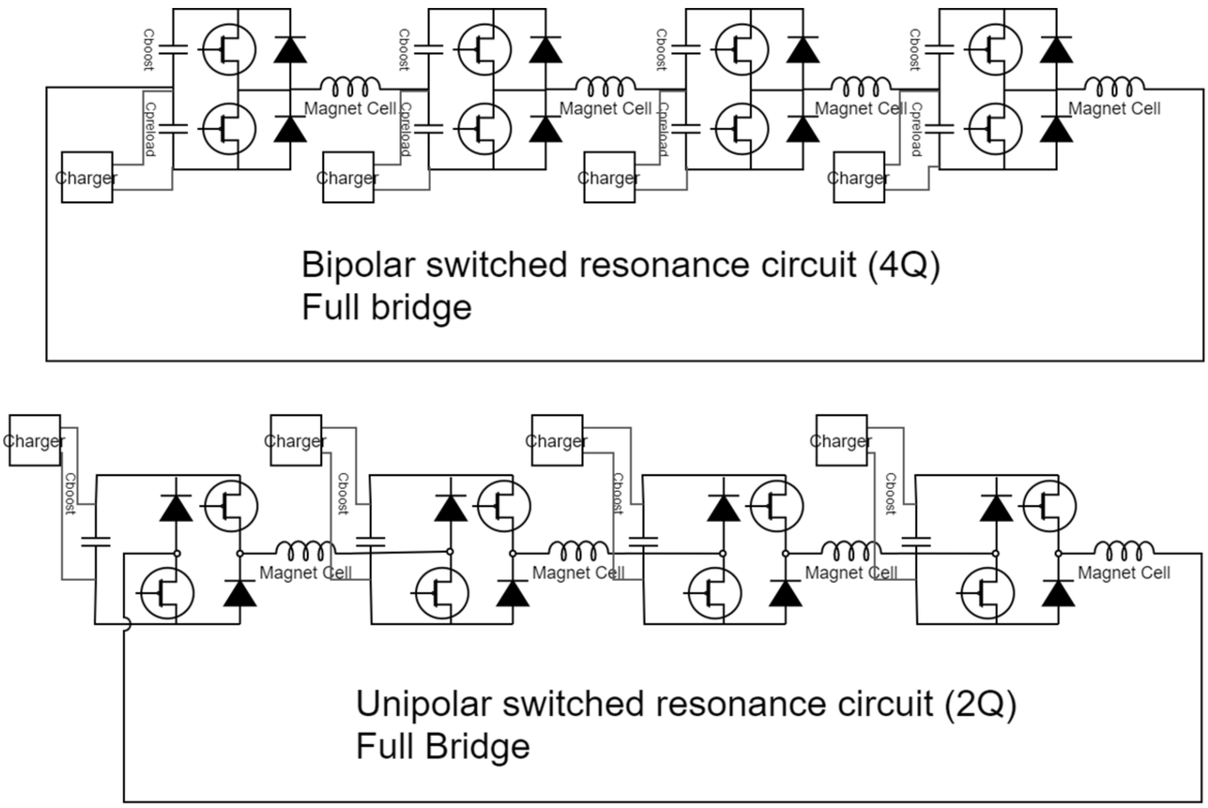

Fig. 6.1.14: Bipolar and Unipolar switched reluctance circuits

hence be in the range of 30 MJ to 120 MJ (considering a dipole filling factor of 0.75). Pulsing these circuits in the range of fractions of ms to ten ms will hence involve managing reactive powers in the range of tens of GW.

Below we describe schematically the powering solution taken as baseline, which includes the crucial component of energy storage, and follow-up with the description of resistive and superconducting magnet optimization and initial engineering design. Further details on power converters optimization and engineering can be found in the dedicated chapter (QUESTION: is this consistent with the rest of the report ?).

6.1.0.12 Powering concept for RCS and HCS and magnet configuration

To power the resistive magnets of RCS and HCS we have chosen a solution relying on resonant power converters and capacitor-based energy storage. This system allows to reach the desired combination of field, aperture and fast ramping, managing efficiently the reactive power. Figure 2 shows the circuits to be used for unipolar or bipolar resonance. The Unipolar resonance is used in case of the RCS configuration (two quadrants), i.e. when only pulsed resistive dipoles are considered, whereas the bipolar circuit is considered for the HCS configuration (four quadrants).

The most complex and challenging configuration is the bipolar one (four quadrant), for which we have performed most of our analyses. As described later, and in detail elsewhere (QUESTION: do we have a chapter on power converters ?) we have scanned extensively design parameters to find optimal configurations that minimize energy storage, reactive and active power, and the need for active filters, which represent one of the most costly systems in the powering scheme.

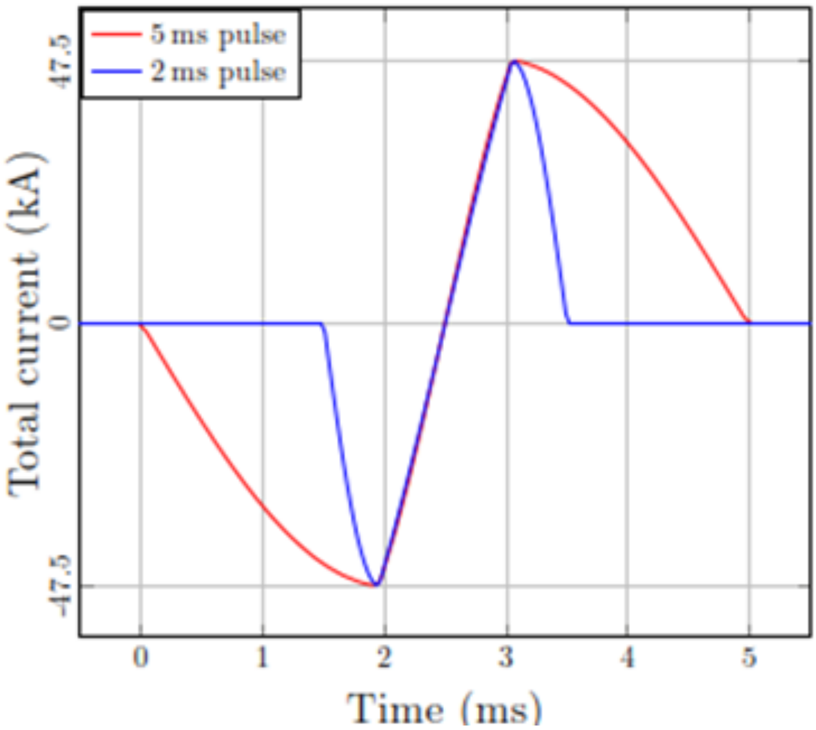

Fig. 6.1.15: Resonant current pulse for dipole magnets

An example of a range of optimal ramps is reported in Figure 1, where we show the requested linear ramp duration (1 ms, from peak negative current to peak positive current), preceded by a "preparation" phase and followed by a "recovery" phase of different duration (0.5 ms to 2 ms). Tuning of this time mainly depend upon the optimization of the power converter design and components, as well as loss (see also later).

The power converter consists of one / two energy storage capacitor bank backed with a reduced power charger and the IGBT/diode discharge leg. Few hundreds of simple circuits called "PEcells" are connected in series with the coils of the dipole magnets interleaved. In order to improve the magnetic efficiency and simplify the design, the dipole magnets will have coils built as single turns (or few turns) to reduce the total inductance, and they will have no heads. The coils will be formed by bars that exit the magnet and traverse the transition till the next PEcell (Figure 3 left) or another magnet is reached (Figure 3 right).

There are two advantages with this connection style:

- There is only one circuit in the full accelerator. No problem of balancing the currents among independent sectors as in the LHC. The ramp-up time is so small that this may be a serious problem);
- The coils are interleaved with the PEcells and with consecutive magnets as well. This would guarantee a relatively small and balanced voltage to ground of all coils and power converters. The approach is like what done in the SPS but with much higher number of circuits.

The baseline circuit configuration described above was used to provide a preliminary evaluation of size and cost evaluation of the magnets and power converters. More details on the powering scheme,

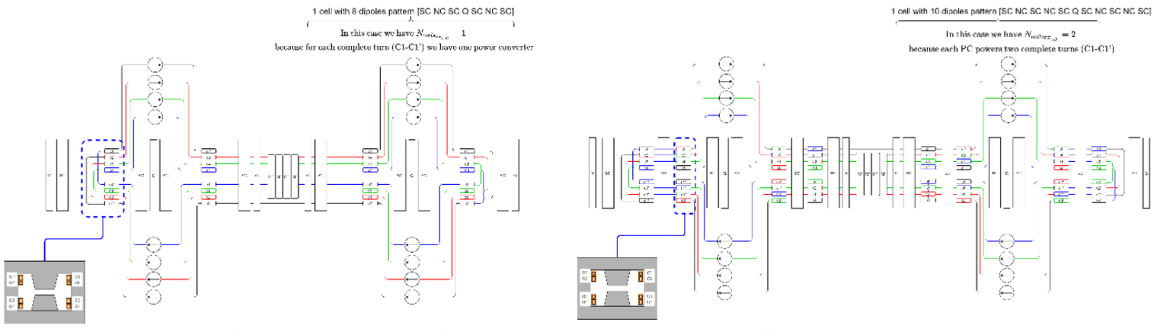

Fig. 6.1.16: Connection between magnets coils and PE cells.

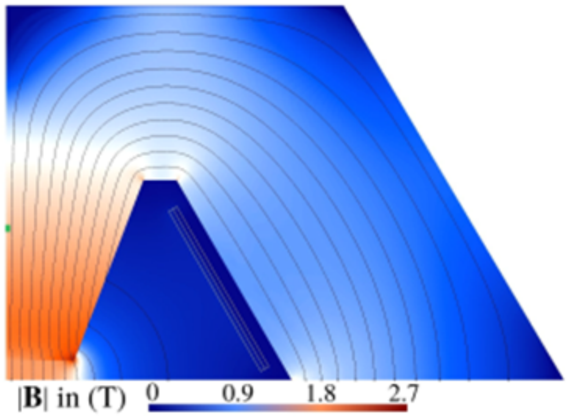

Fig. 6.1.17: MAP design with increased coil length and gap dimensions 30x100mm

optimization and technical solutions are reported in the chapter on power converters (QUESTION: which chapter, and proper reference ?).

6.1.0.13 Resistive dipole magnet

As for other areas of magnet design, we have started from the results of the US-MAP study. The US-MAP resistive dipole was designed for a bore field of 1.5 T and an aperture of 25 mm (H) x 156 mm (W). The stored energy of this dipole has been calculated at 4.2 kJ/m, and the total loss per cycle, assuming a 1 ms cycle is 112 J/m (see later for details). If we modify the design to meet the IMCC RCS and HCS specifications of 1.8 T in a 30 mm (H) x 100 mm (W) aperture, as shown in Figure 5, the stored magnetic energy rises substantially to 7.08 kJ/m, and the total loss per cycle is also much increased to 277 J/m. Assuming a 5 Hz repetition rate, this loss per cycle corresponds to 1.385 kW/m.

We have then explored alternative designs. The analysis performed mainly aimed at limiting the magnet stored energy, as this limits the reactive power required from the power converter during fast ramps and reduces the size of the energy storage. To investigate optimal magnet configurations for the RCS resistive dipole magnets, three geometric designs were considered, namely the hourglass [10], the window-frame [11], and the H-type [11, 12]. The best configurations found are shown schematically in Fig. M4. These configurations were optimized to minimize stored energy, subject to the constraint of achieving a specified magnetic flux density in the magnet air gap. The optimization procedure involved varying the peak engineering current density in the coils from 10 to 20 A/mm². The optimization uses

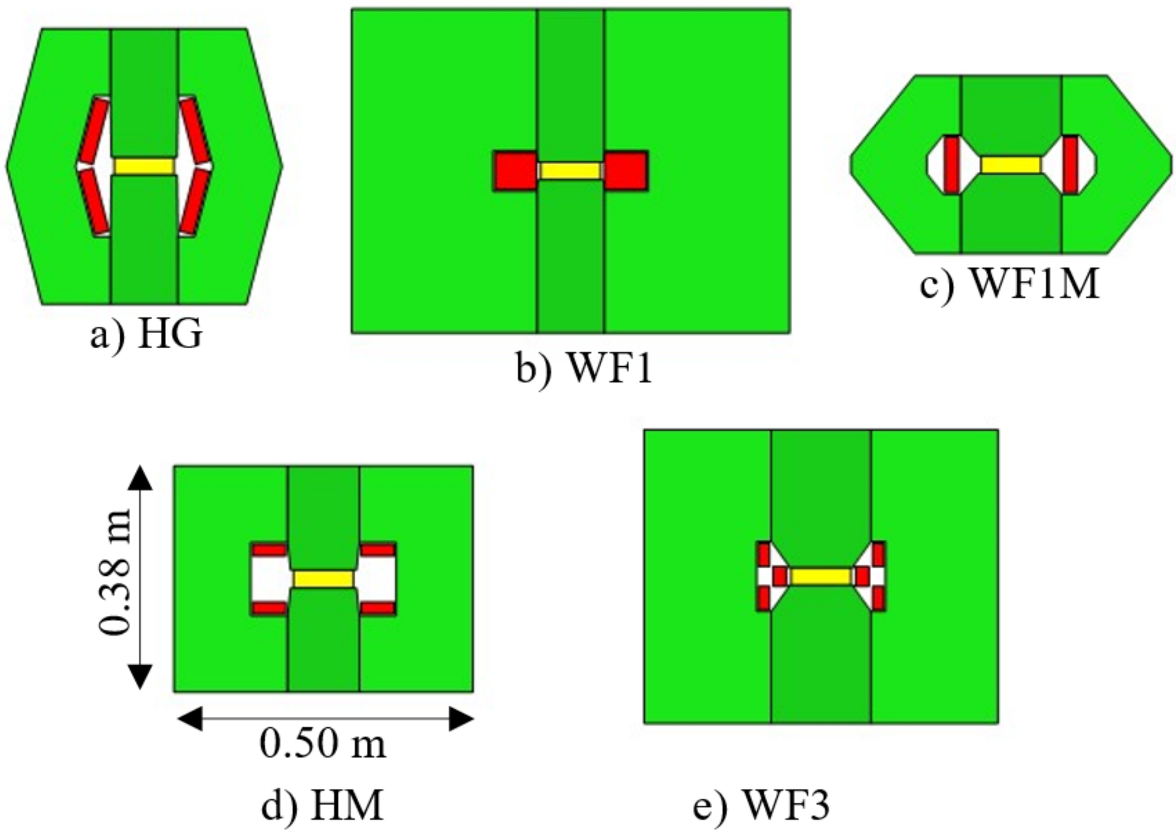

Fig. 6.1.18: Summary of the optimized geometries (the cross sections are to scale): a) Hourglass, J = 10 A/mm2, b) Window-frame WF#1, J = 10 A/mm2, c) Window-frame WF#1M, J = 20 A/mm2, d) H-type HM, J = 20 A/mm2; e) Window-frame WF#3, J = 20 A/mm2.

an interactive routine based on Matlab for the optimizer part and FEMM for the 2D magnetic field and loss analysis. The routine scans geometric and electric variables and computes the electromagnetic field, searching for the configuration with minimum cost function which is a weighted sum of stored energy, difference from the specified 1.8 T bore field, and field errors [paper from Marco].

Two commercial ferromagnetic materials were selected for the resistive dipole's magnetic circuit: Supermendur for the pole pieces and M22 steel for the remainder of the yoke. Supermendur exhibits a high magnetic permeability up to 2.0 T, which is advantageous for minimizing the total ampere-turns and the Joule losses in the conductor. Its linear magnetic characteristics also determines a reduction of the iron losses during rapid field transients. However, Supermendur contains Cobalt, which may get activated in a strong irradiation environment. M22 steel, while less permeable, is more cost-effective, radiation-resistant, and suitable for lateral yoke branches where lower magnetic flux densities are present.

Among the different analyzed configurations, the Hourglass (HG) and H type magnet (HM) exhibit the best results both in terms of stored magnetic energy and losses. Specifically, the HG dipole has stored magnetic energy of 5.77 kJ/m, and total loss per cycle of 406 J/m. This corresponds to an average power loss of 2.03 kW/m. The HM dipole has stored magnetic energy of 5.74 kJ/m, and total loss per cycle of 423 J/m, which corresponds to an average power loss of 2.12 kW/m. In both cases, as done earlier, we have computed the average loss assuming a pulse repetition frequency of 5 Hz. The values for HG and HM dipoles are very close, but, while the stored energy is much smaller than the US-MAP dipole adapted to the IMCC specifications, the loss is much larger. This is because the US-MAP design allows for a larger conductor window, reducing resistive loss at the expense of a larger magnetic circuit, and correspondingly larger stored magnetic energy.

For a final comparison, it is also interesting to consider the SPS dipole, which has similar gap dimensions and maximum bore field. The SPS dipole has a stored magnetic energy of 19 kJ/m, over three times that of the optimized muon collider accelerator dipoles. The reactive power is 6.8 kW/m, also three times higher than projected for the muon collider accelerator dipoles, though in this case we need to recall that the SPS is operated continuously at low frequency while the RCS have a duty cycle of less than 5 % but with current frequency of the order of 500 Hz. Still, this comparison demonstrates that the optimization was very effective in reducing both active and reactive power, as well as energy storage needs.

In this initial magnet optimization step the resistive losses were not part of the cost function, and the optimizer always tried to reduce the magnetic circuit area as much as possible. While this is surely advantageous for the power converter, it may not be the best solution and losses in the conductors may be too high. We will come back later on this, showing how this is adderssed.

To speed up the calculation of the magnetic field produced by the resistive dipoles, an alternative method to the FEMM simulation was developed and applied to the analysis of the H-magnet configuration. This method is based on an equivalent lumped parameters non-linear magnetic circuit of the resistive dipole. The topology of the magnetic circuit is obtained from the geometry of the magnetic configuration. The introduction of magnetic reluctances at given locations of the magnetic circuit is based on the analysis of the flux lines obtained through 2D simulations performed with FEMM. An example of magnetic circuit obtained is shown in Fig. 2.10. The reluctances of the ferromagnetic structure are computed accounting for the non-linear characteristics of the magnetic materials used for the difference parts of the structure itself, namely Vacoflux 48 for the poles and the M235-35A for the yoke. The magnetic circuit obtained is then solved by means of the mesh analysis.

The magnetic circuit method has a very good accuracy for a first assessment of the resistive dipole design, with errors on field, stored energy and losses within few %, with a substantial reduction of the computation time. To give orders of magnitude, the computation time of a magnet configuration drops by more than two orders of magnitudes compared to 2D FEM, from minutes to seconds.

6.1.0.14 Magnetization, resistive and eddy currents losses

Losses in the resistive magnets are one of the main concerns in the design of the dipoles, as can be inferred from the evaluation of losses reported in the previous section. In fact, evaluating the loss in the specific conditions of the RCS and HCS is not trivial. Losses originate from magnetization hysteresis and eddy currents in the iron laminations, and resistance in the copper coils. Iron losses are well understood within classical electrical engineering. In our case the challenges are the specific geometry and end effects, the fact that the iron is saturated in a large portion of the yoke, and the fact that the database of loss in the frequency regime of interest, about 1 kHz, is not as established as would be necessary. For the copper coils, the frequency is such that the skin depth is in the range of mm. A single conductor bar would not be fully penetrated during a pulse, and the skin current would result hence in much higher

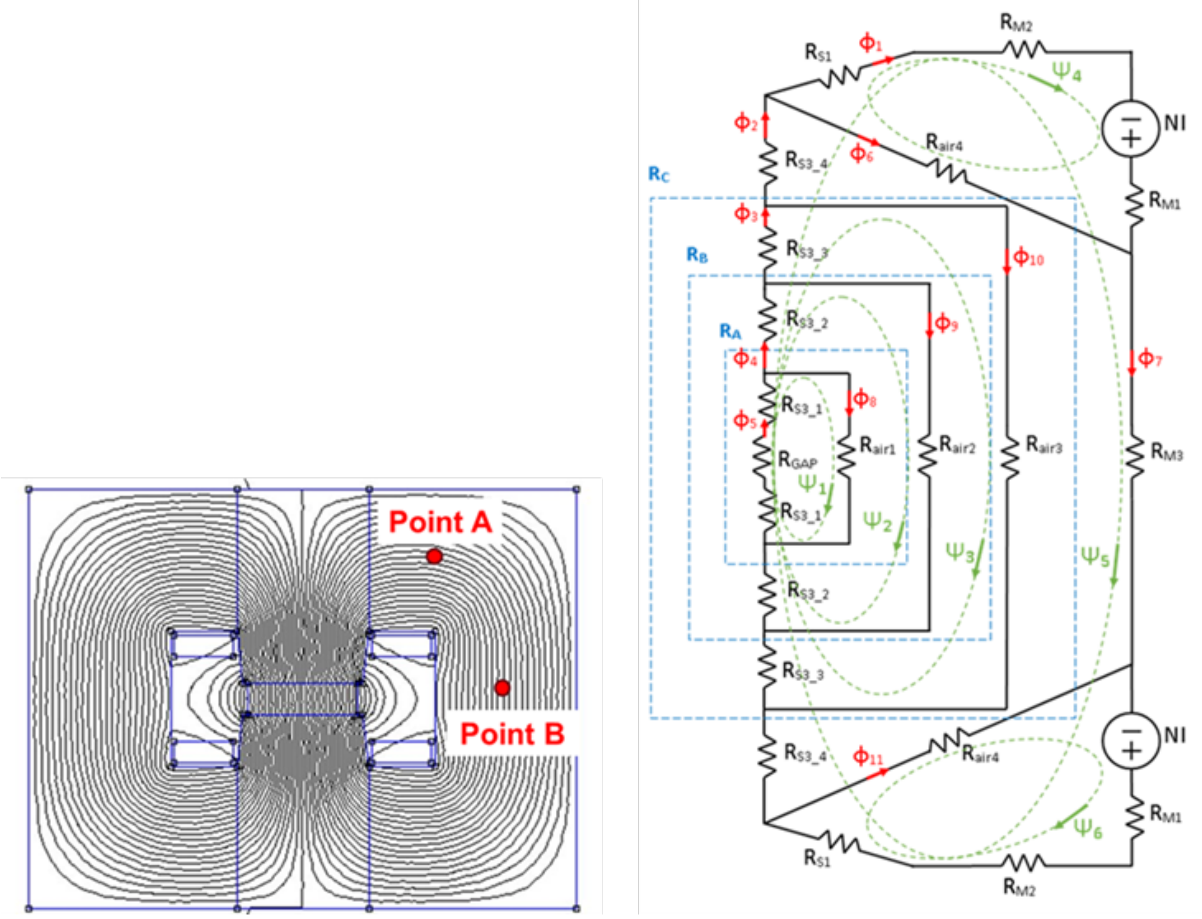

Fig. 6.1.19: a) Magnetic flux density map of the H-type dipole and b) corresponding equivalent magnetic circuit. The magnetic flux density calculated in Point A and Point B is used as a reference for the validation of the results of the circuit model.

resistive loss than would be the case for uniform current distribution. This requires appropriate design devices to drive current distribution in the copper conductors.

Given the challenge, we have performed some benchmarking of loss evaluation using different numerical and semi-analytical transient simulation methods, taking the design values from US-MAP as a starting point. The US-MAP resistive dipole was designed for a bore field of 1.5 T and an aperture of 25 mm (H) x 156 mm (W). This has been reproduced using Maxwell 2D and proprietary software at the Technical University of Darmstadt. The magnet geometry in the latter case was slightly modified to allow for higher field, 1.8 T as specified for the IMCC RCS and HCS. The result of the loss calculation are reported in Tab. 6.1.6, where the various components and total loss are given. A cycle of 1 ms was assumed for the calculations. We see from the figures reported there that there is consistency of values, but the spread is significant, typically ± 20% around the average of all results. Experimental data would be necessary at this stage to progress further.

An example of loss evaluation is shown in Fig. 6.1.18, where we show the influence of the preparation and recovery phases of different length outlined in Figure 1, applied to the magnet design in Fig. XXX (US-MAP) The total loss, iron and coil, depends on the total duration of the cycle, and we see from Fig. XXX that there is a clear advantage in maintaining the total cycle time, including preparation and recovery, as short as possible. This result is rather trivial, powering for longer time increases Joule

ANALYSIS	US-MAP	Maxwell 2D	TUDa	TUDa
Bore field (T)	1.5	1.5	1.5	1.8
Aperture (mm x mm)	25 x 156	25 x 156	25 x 154	25 x 154
Stored energy (kJ/m)	4200	4900	4551	6644
Static loss per cycle				
Iron yoke (J/m)	33	59	21.8	32
Iron pole (J/m)	63	61	40.8	58.5
Coil (J/m)	16	33	17.8	31.5
Dynamic loss per cycle				
Coil (J/m)			25	37
Total loss per cycle (J/m)	112	153	105	158

Table 6.1.6: Benchmark of loss calculations for the geometry of the resistive dipole defined by US-MAP. Calculations for 1.5 T [338] and 1.8 T (reference IMCC design). A cycle time of 1 ms is assumed.

heating. What cannot be seen by such an analysis is the effect on the power converter, which has added complexity and cost when demanding faster ramps. We expand on this next.

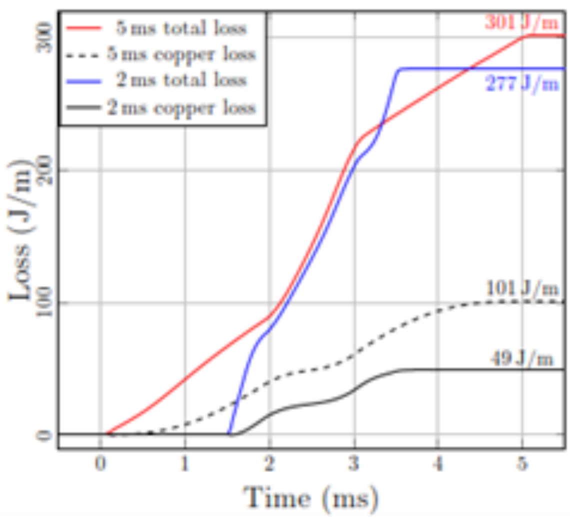

Fig. 6.1.20: Resistive and total loss evaluation for two cycle alternatives with the same ramp time of 1 ms, but either 2 ms or 5 ms total time, see Fig. 6.1.14. The geometry of the modified US-MAP dipole, see Fig. XXX, was used for this calculation.

6.1.0.15 Global optimization and specifications for power converter

It should be clear from the discussion so far that it is not possible to design an optimal resistive dipole circuit by separately optimizing for the various components and issues. This is why we have created a combined optimizer model of the magnet and the power converter, and used this model to study several optimization directions towards minimal the capital and operational expenditures (CAPEX and OPEX).

The model considers a dipole magnet with a generic geometry inspired by the US-MAP Hourglass concept. This was shown in the dipole optimization exercise reported above to be one of the best configurations, so representative for global optimization purposes. The optimizer is presently based on the magnetostatic and harmonic solver in FEMM, for the magnetic sizing and evaluation of copper conductor losses. Similar to the effort on the reluctance based magnetic model described earlier, an

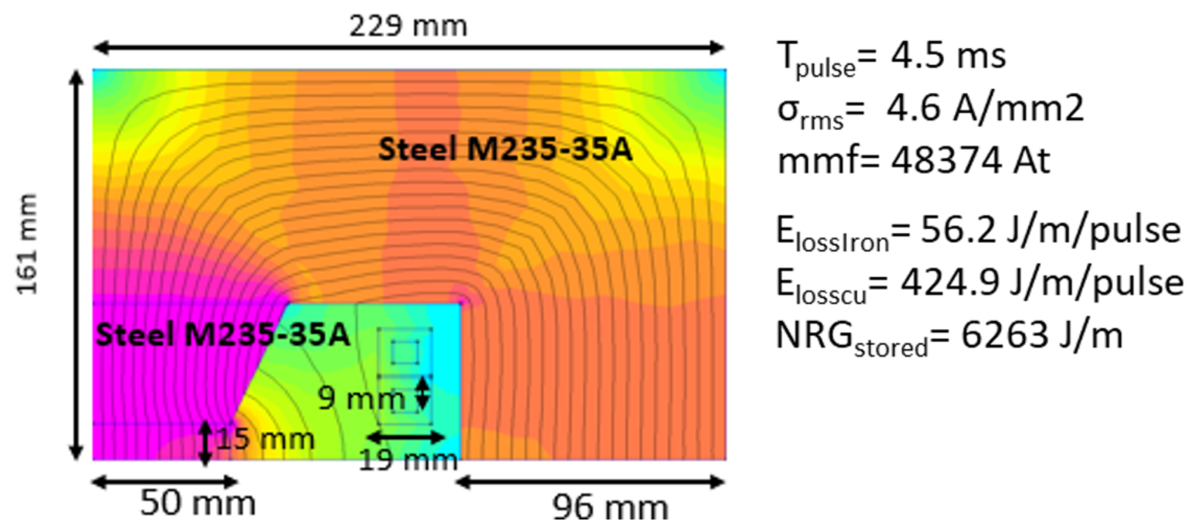

Fig. 6.1.21: Result of CAPEX+OPEX optimization on the dipole

Artificial Neural Network (ANN) model for the identification of losses in conductor without the need to run the finite element code is under development. Additional design features important for the design of the power converter have been added, like the possibility to have coils made by parallel conductors and cooling holes in the conductor.

An example of global CAPEX+OPEX optimum reached by this method is reported in Figure 7. When operated at 1.8 T with a magneto-motive force of 48.4 kA turn, the dipole schematically shown there has a stored energy of 6.24 kJ/m. This is larger than the optimum value found from the stand-alone dipole optimization, by 10 %. Losses per cycle are 481 J/m, originating in large part from the resistive loss in the coil (425 J/m) and only marginally from the iron (56 J/m). This is also larger than the values found by optimizing the dipole alone, by nearly 20 %. Including holes for water cooling, thus reducing the copper cross section, increases the losses in conductors. Finally, the pulse time that corresponds to the lowest CAPEX and OPEX is relatively long, 4.5 ms, which is counter-intuitive in the light of the higher resistive loss for longer powering time. In terms of total CAPEX and OPEX this is offset by the reduced demands on the powering side. This result demonstrates the need of performing optimization at system level, as just focusing on the magnets does not produce a minimum cost solution.

The result of the global optimization can finally be used to yield design specifications for the power converters and energy storage units. The linear inductance computed using the ratio of energy and conductor current results in a value of:

$$L = \frac{2E_{stored}}{I^2} = \frac{2 * 6263}{(48374/4)^2} = 85H/m \tag{6.1.1}$$

And the average resistance is given by:

$$R = \frac{E_{loss}}{T_{pulse}I^2} = \frac{(56.2 + 424.9)}{0.0045(48374/4)^2} = 650\mu Ohm/m \tag{6.1.2}$$

These values are used for determining the size of the power converters. In fact, these are conservative values. Because the iron saturates, the total energy to be switched by the power converter is

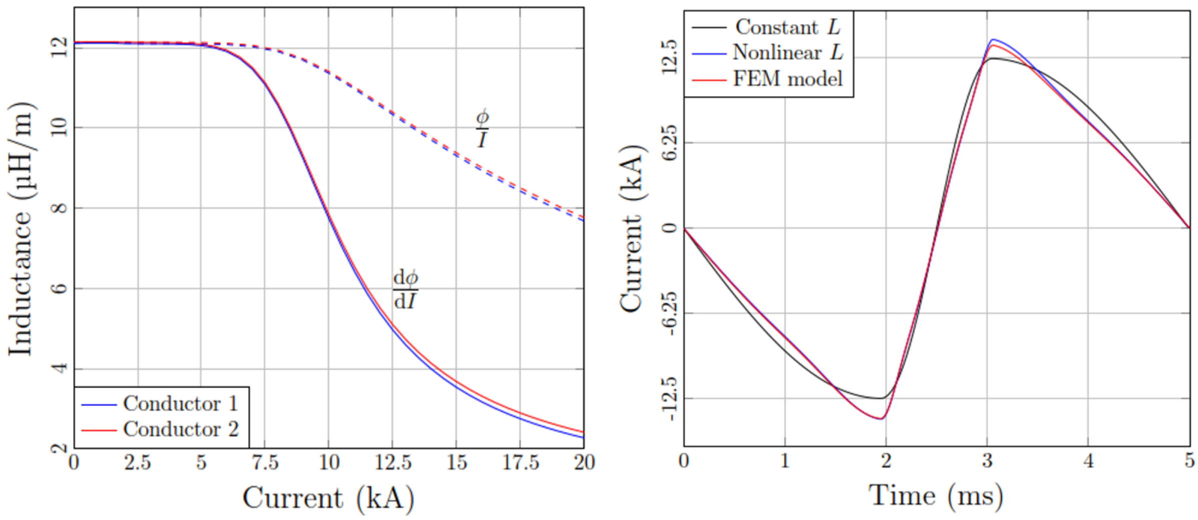

Fig. 6.1.22: Circuit-Magnet transient simulation

overestimated. This is shown by the detailed analysis reported in Figure 8, where we have evaluated the actual non-linear inductance and its differential (right), and its effect on the current ramp (left). The current transients obtained with a constant value of inductance (black curve) is significantly faster than the values obtained with non-linear inductance (red and blue curves). Non linear differential inductance should be considered to avoid excessive design margins.

6.1.0.16 Resistive quadrupole magnet

A similar study to the one performed to identify the most suited dipole magnet configuration was conducted for the quadrupole magnet design. Four configurations were analyzed to understand which could better reduce the power losses, the magnetic energy stored, or both. The quadrupole magnets were designed to have a field gradient of 30 T/m and a specified field quality of 10^{-4}.

The four configurations were optimized for three values of the air gap diameter, 40 mm, 60 mm and 80 mm, and were compared in terms of total losses, real and reactive power absorbed and stored magnetic energy. A synoptic view of optimal configurations for a bore aperture of 60 mm is shown in Fig. 6.1.23. The most suitable configuration to reduce the losses is the configuration proposed by US-MAP, configuration 1 in Fig. 9. For a bore aperture of 60 mm, this configuration has a stored energy of 2.4 kJ/m and an average power loss of 212 W/m. The best alternative is the configuration with trapezoidal coils, and smallest magnetic circuit, configuration 4 in Fig. 9. For a bore aperture of 60 mm, this configuration has a stored energy of 0.83 kJ/m and an average power loss of 352 W/m.

All the optimized configurations achieve the specified field gradient of 30 T/m. However, none of them is yet able to satisfy the field quality requirement. Therefore, further investigations are required to improve this aspect of the quadrupole design.

6.1.0.17 Superconducting dipole magnets

In parallel to the work on the normal-conducting pulsed magnets, we are progressing with the design of the superconducting magnets of the hybrid cycled synchrotrons (HCS). These magnets provide a field offset, and allow using the full field swing of the normal conducting magnets, from negative to

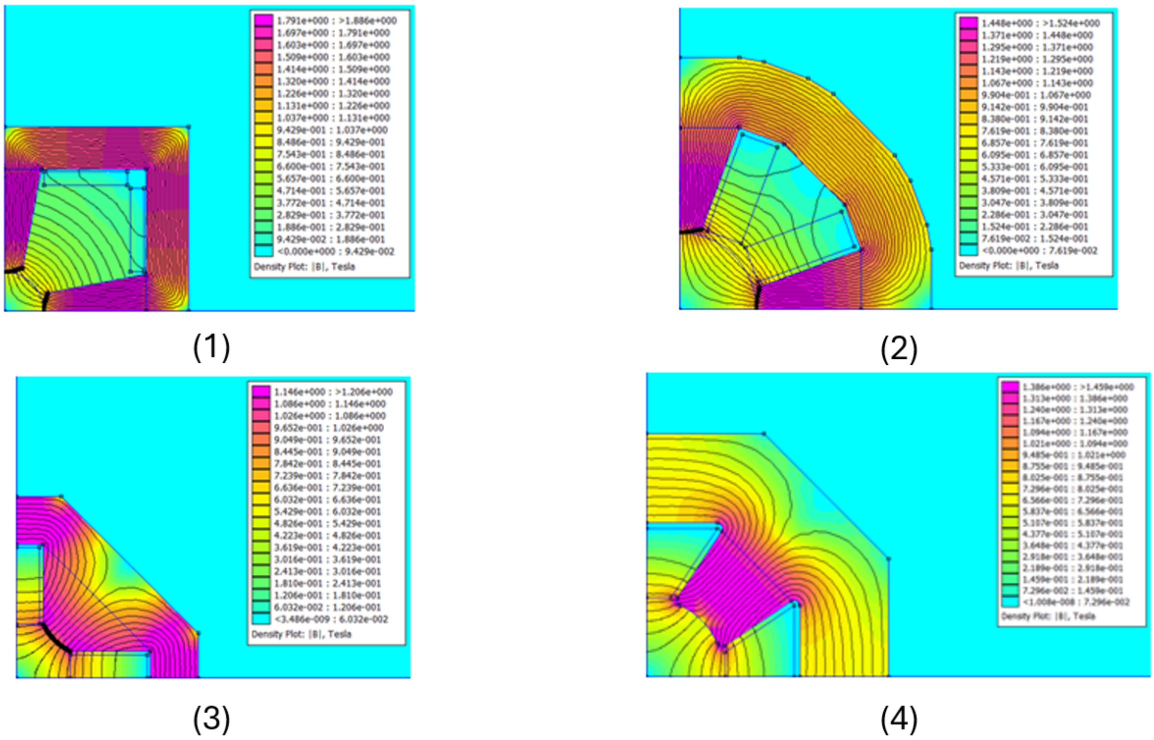

Fig. 6.1.23: Optimized quadrupole configurations for a bore aperture of 60 mm.

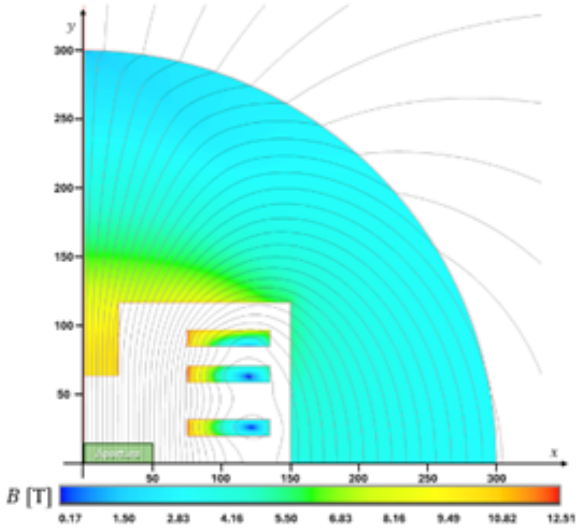

Fig. 6.1.24: Conceptual design of a 10 T HTS, 30 mm x 100 mm aperture dipole for the hybrid cycled synchrotrons.

positive field values, effectively making the synchrotrons shorter. The work has focused on HTS dipoles, operated in gaseous helium (10 K to 20 K) generating a 10 T steady state field in a rectangular aperture identical to that of the resistive dipole magnets, i.e. 30 mm x 100 mm. The choice of HTS was driven by the intent to have a large operating margin and reduce consumption, especially in light of the effect of the bursts of muon decay that will cause periodic heating of the magnets. Also, operation at temperature significantly higher than liquid helium will ease the engineering of the transitions from resistive to superconducting magnets that takes place in each cell.

Following initial conceptual studies, the configuration presently studied in detail is shown in Fig. M5. The geometric requirements for this dipole have led to a design featuring six planar racetracks, three above and three below the midplane. To simplify both the mechanical structure design and the assembly process, each racetrack consists of 205 turns, and all are perfectly aligned. The magnetic design includes a circular iron yoke that surrounds the coils. The yoke has an outer radius of 300 mm and an inner square window, optimized to maximize magnetic performance and field quality while ensuring at least 30 mm of clearance between the racetracks and the yoke to accommodate the mechanical structure. Additionally, the yoke features a pole with dimensions optimized to further enhance the field quality. The field quality requirements specify that all harmonic components must remain below 10 units within a good field region of 50 mm × 20 mm. Field quality has been assessed using two methods: the first involves four harmonic expansions, each with a 10 mm radius, positioned at x = 0 mm, 5 mm, 15 mm and 25 mm; the second method uses four paths to calculate the field magnitude from x = 0 mm to 25 mm, evenly distributed in y between 0 mm and 10 mm. This design largely meets all field quality requirements: all harmonic components range between -4.5 and 0 units, achieving a field homogeneity of 0.03%. The Table below reports all the main parameters of the optimized design of the dipole.

Parameters	Value
Central field	10 T
Peak field	12.51 T
Current	2314 A
Engineering current density	714 A/mm^2
Margin on loadline	25.7%
Operating temperature	20 K
Temperature margin	2.5 K
Magnetic length	1.3 m
Mechanical length	1.6 m
Iron yoke radius	300 mm
Number of racetracks per quadrant	3
Number of turns per racetrack	205
Number of HTS tapes per turn	2
Inductance	1.3 H
Stored energy	2.24 MJ

Table 6.1.7: Main parameters of the optimized design of the dipole.

The mechanical analysis was conducted using an ANSYS APDL macro, where Lorentz forces were imported node by node from the electromagnetic model. The simulation includes an infinitely rigid structure surrounding the racetracks, with stainless steel cases having an inner over thickness of 0.1 mm. This additional thickness allows the racetracks greater freedom to deform under the influence of Lorentz forces, preventing over constraining of the conductors and yielding more realistic results. The peak Von Mises stress, with a value of 172 MPa, occurs at the lower left corner of the first block. It is notable that the net force in the y direction on the first block is positive (upward). This outcome, which was a secondary goal of the magnetic optimization, facilitates structural designs that keep the midplane region clear, reducing heat deposition from radiation in components likely to be in direct contact with the superconducting material. Given that most of the mechanical load arises from the x component of the Lorentz forces, a stress management strategy has been implemented and optimized to address these forces effectively. The baseline configuration was improved by introducing a 5 mm thick septum, modeled as infinitely rigid, consistent with the rest of the structure. The position of each septum was individually optimized, resulting in slight variations in the number of conductors on either side of the septum across different blocks. This modification reduced the peak Von Mises stress by half, down to 85 MPa. The adjustment to the cross-section has minimal impact on magnetic performance: compared to the baseline configuration, the required current is 2% higher, the peak field is 1.4% lower, the new load line margin is 22.8%, and the stored energy increases by 5%. Furthermore, all harmonic components remain within the range of -2 to 2 units, with a field homogeneity of 0.04%.

QUESTION: Mention pulsed HTS dipoles as an option for the last RCS ?

6.1.0.18 Challenges identified

As we anticipated, the main perceived challenge for the RCS and HCS magnets is the aspect of system optimization. It is the mainly interplay of magnet design, energy storage and power conversion that needs to be understood and mastered to yield finally to an optimal global design. We have directed our main efforts in this direction, towards a baseline design that will result in minimum CAPEX and OPEX. Still, there is a definite need to:

- Demonstrate pulsed dipole circuit performance in conjunction with energy storage and power conversion, validating the tracking of ramp current and field reference, the evaluation of losses, the energy recovery efficiency, as well as transient field quality. Such demonstration should be also relevant to the large number of pulses planned throughout the lifetime of the accelerator.

At the same time, there are technical aspects that deserve special attention, namely:

- Hysteresis, eddy current and coil resistive losses in the regime of frequency of interest, specific to the resistive magnets of the RCS and HCS. We believe that for this the magnetic material database is not sufficient for accurate prediction;
- Field quality in pulsed magnets, especially in presence of other magnetic and/or conducting components (e.g. beam pipe) which will affect field lags and time constants;
- Demonstration of accelerator-level performance, specific to the superconducting HTS dipoles of the HCS. This challenge is shared with that of the collider magnets.

Collider magnets

The magnets in the collider are the final big challenge that we have identified. Besides the difficulty in the magnet technology, muon beams require optics solutions that are far from standard practice, and integrating the specifications from beam optics poses an additional challenge. In order to provide quick feedbacks to the beam dynamics, cryogenics and energy deposition study requirements, an analytic evaluation of the maximum magnet performances as a function of the magnet aperture was performed (see [339] and [340]). This preparatory work has then led to the choice of specific design points for the main dipoles and IR quadrupoles of the collider, which we have used to initiate conceptual and engineering design of the collider magnets. We describe below the results of this work.

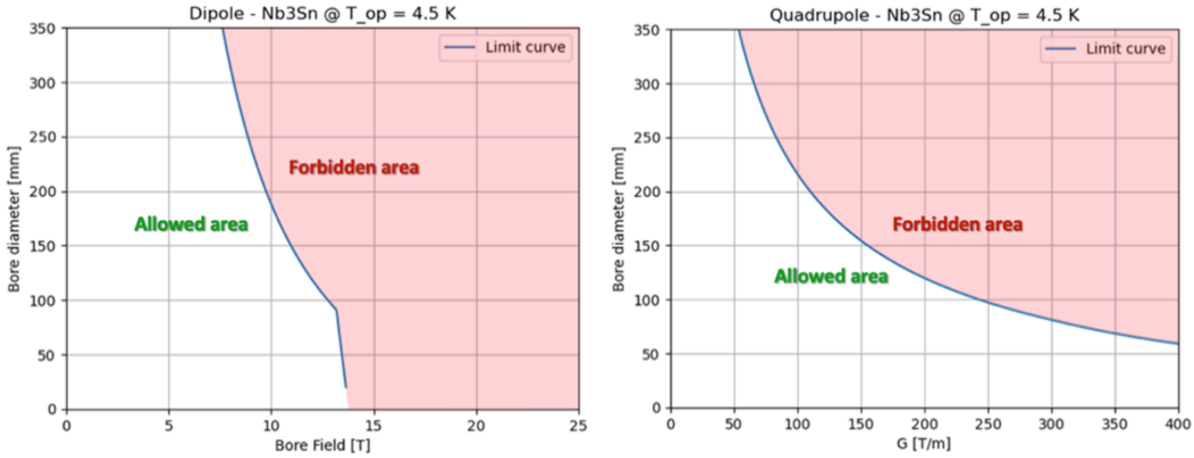

Fig. 6.1.25: A-B plot for dipoles and A-G plot for quadrupoles built with Nb3Sn and operated at 4.5 K.

6.1.0.19 A-B plots

To evaluate the maximum dipolar field or quadrupolar field gradient obtainable, a sector coil approximation was assumed and all the most important constraints were included in the calculation, namely:

- Margin on the load line. A temperature margin of 2 K was assumed for NbTi, while 2.5 K was considered for Nb3Sn and ReBCO. While in the case of Nb3Sn the margin is required to ensure stable operation and limit training, in the case of ReBCO we would expect that such margin would be largely more than what is needed. However, considering that we plan to design for operation in gas, we have kept the same margin to accommodate for temperature fluctuations that may come from the cryogenic system.
- Feasibility of the protection system. A 40 ms time delay between the quench and the firing of the protection system were assumed and a maximum hot-spot temperature at the end of the discharge of 350 K for NbTi and Nb3Sn and 200 K for ReBCO were set, as explained in details in [339].
- Mechanics: the average stress on the midplane was estimated analytically considering only the E.M. forces as explained in [339] and the limit was set to 100 MPa, 150 MPa and 400 MPa respectively for NbTi, Nb3Sn and ReBCO.
- Cost: the target budget was set to 400 kEur/m for the arc magnets, more than twice the limit set for the FCC project [ref], and 800 kEUR/m for the IR magnets considering the total dimension of the collider ring and available budget for the entire accelerator complex.

The result of this analysis are "A-B" plots of maximum aperture for a given field, and "A-G" plots of maximum aperture for a given gradient, satisfying all requirements above. We report in Figs. M6 (A-B and A-G plots for Nb3Sn operated at 4.5 K, 400 kEUR/m cost limit), Fig. M7 (A-B plots for REBCO dipoles operated at 4.5 K, 10 K and 20 K, 400 kEUR/m cost limit) and Fig. M8 (A-G plots for REBCO quadrupoles operated at 4.5 K, 10 K and 20 K, 800 kEUR/m cost limit).

For NbTi, the same analysis performed for other superconducting materials has been carried out. While this material does not achieve the required performance for a 10 TeV collider, it remains a viable alternative for a 3 TeV collider and provides an excellent reference for the work performed. Figure M10

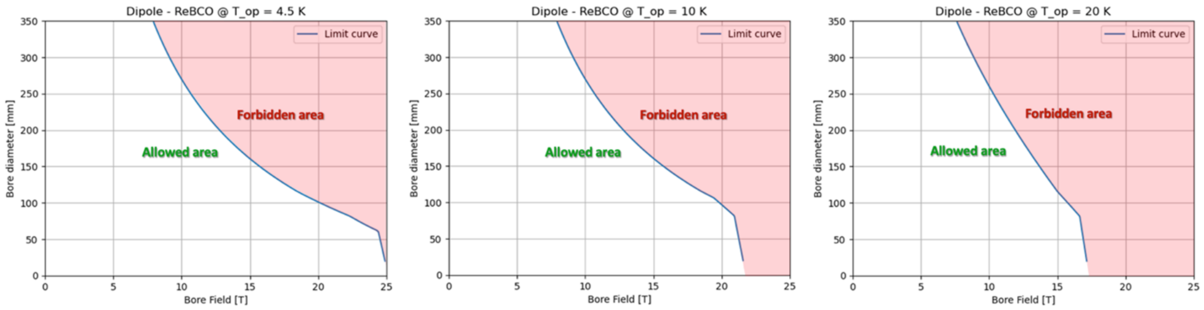

Fig. 6.1.26: A-B plot for dipoles built with REBCO and operated at 4.5 K, 10 K and 20 K.

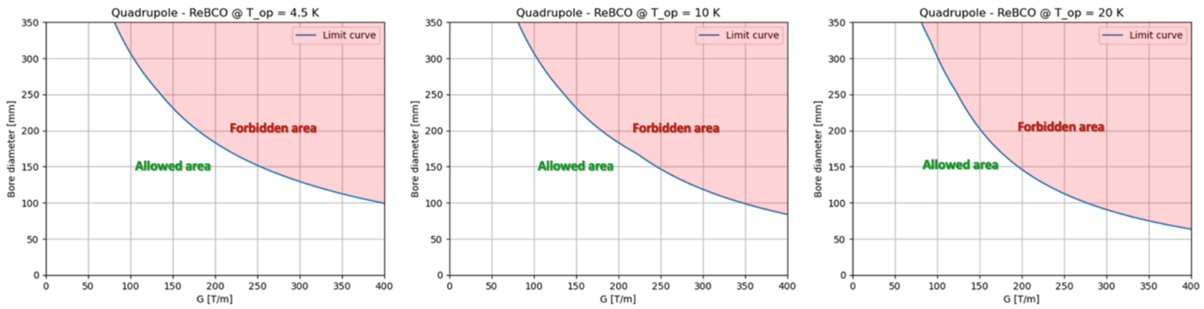

Fig. 6.1.27: A-G plot for quadrupoles built with REBCO and operated at 4.5 K, 10 K and 20 K.

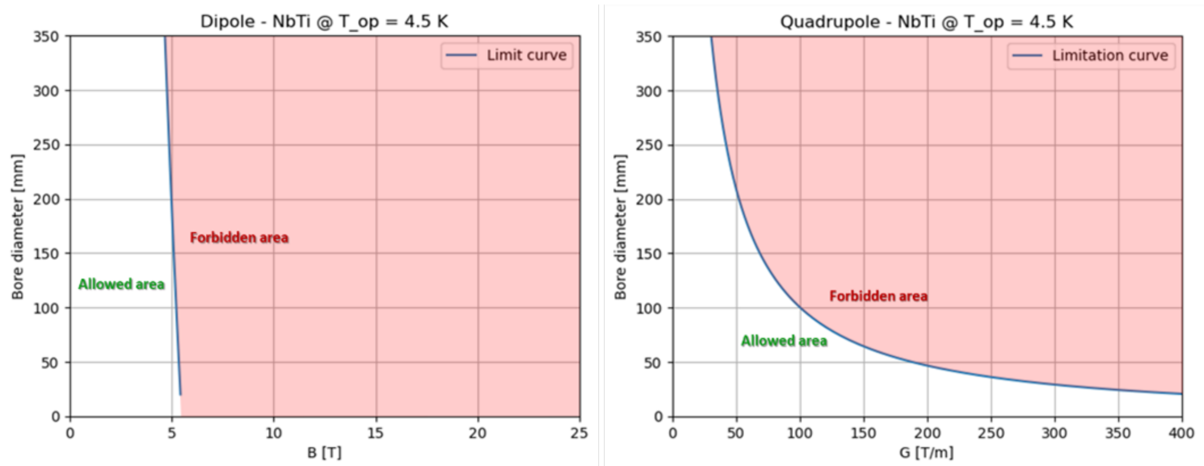

Fig. 6.1.28: A-B plot for dipoles and A-G plot for quadrupoles built with NbTi and operated at 4.5 K.

shows the A-B and A-G plots for NbTi magnets, assuming an operating temperature of 4.5 K.

Using the data presented in the plots, additional performance limits for combined-function arc magnets have been derived, illustrating the maximum achievable combination of dipolar field and quadrupole gradient as a function of the magnet bore aperture (see Figure M9). The results are based on a nested magnet configuration, with the quadrupolar coil positioned within the dipole bore. Also in this case the reported performance limits satisfy the constraints of maximum cost minimum temperature margin, and the maximum mechanical stress on the conductor.

The minimum aperture of the arc dipoles have been obtained from considerations of beam optics, impedance, radiation shielding, cryogenics and vacuum integration. In particular, the magnet aperture in the collider arc needs to be at least 158 mm for a cold mass at 4.5 K and 138 mm for a cold mass

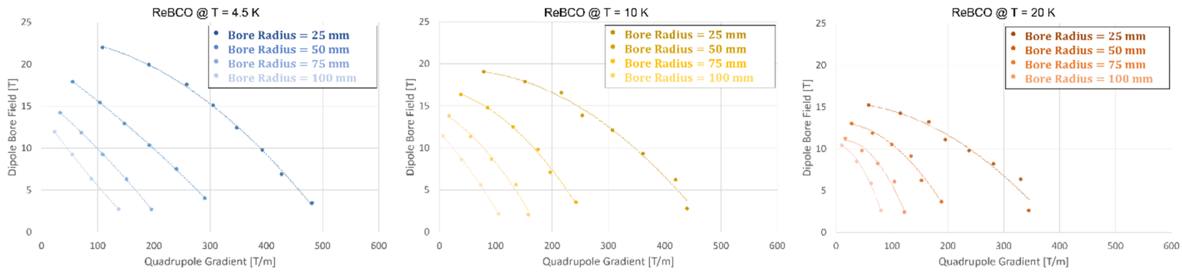

Fig. 6.1.29: B-G plots for nested combined dipole and quadrupoles with REBCO conductor operated at 4.5 K, 10 K and 20 K.

at 20 K. Using the above plots, we see that a dipole built with Nb3Sn, with an aperture of 158 mm, operated at 4.5 K, can reach fields of the order of 11 T. The same evaluation of a dipole built with REBCO, with an aperture of 138 mm, operated at 20 K, can reach fields of 14 T. We have hence set these as magnet performance targets representative of the challenges and pushing the limit of present technology. We note at this point that these magnet performance targets imply dipole coil dimensions that are significantly larger than what has been done in HL-LHC, and what is planned for FCC. Typically, the stored energy is a factor three to four larger. For the 3 TeV stage, using Nb-Ti at 4.5 K, a field of 5 T appears within reach.

The quadrupole performance limits are especially crucial for the IR, which is a major challenge of a muon collider. We see from the plots above that the performance limits follow an approximate A = Bpeak/G dependence, where the parameter Bpeak is approximately 5 T for Nb-Ti, 10 T for Nb3Sn and 15 T for REBCO. The quadrupole magnets used in the present IR 10 TeV optics scale with a similar dependence, and we argue that developing a quadrupole of this class would be relevant to the whole IR. In this case we can focus on the largest gradient magnet, 300 T/m, which requires an aperture in the range of 140 mm.

Finally, we see that when considering combined function dipole-quadrupole magnets the magnet performance is limited by the interaction of the two fields, as expected. Using the results reported above, we see that targeting a field of 14 T, and operating at 10 K to have some additional margin, we can only reach an additional field gradient of 100 T/m. Further iterations with beam optics are necessary at this stage, to integrate the results of this study.

To the best of our knowledge these results represent a truly novel approach to magnet design, which was not formalized earlier. The above plots define performance limits of all main accelerator magnets with unique clarity. Still, we recall that the above performance limits should be taken only as guidelines for the choice of parameters combination. Indeed, being purely analytical, they are powerful scaling and scoping tools, but cannot substitute for actual engineering design which may require additional margins to cope with actual geometric and material constraints, or may offer optimization windows that allow exceeding the analytical scaling, see below.

6.1.0.20 Conceptual design of dipole options

Starting from the analytical evaluation described above, we have initiated a detailed FEM-based design work on REBCO dipole magnets. The aim is to address critical aspects of implementing this technology

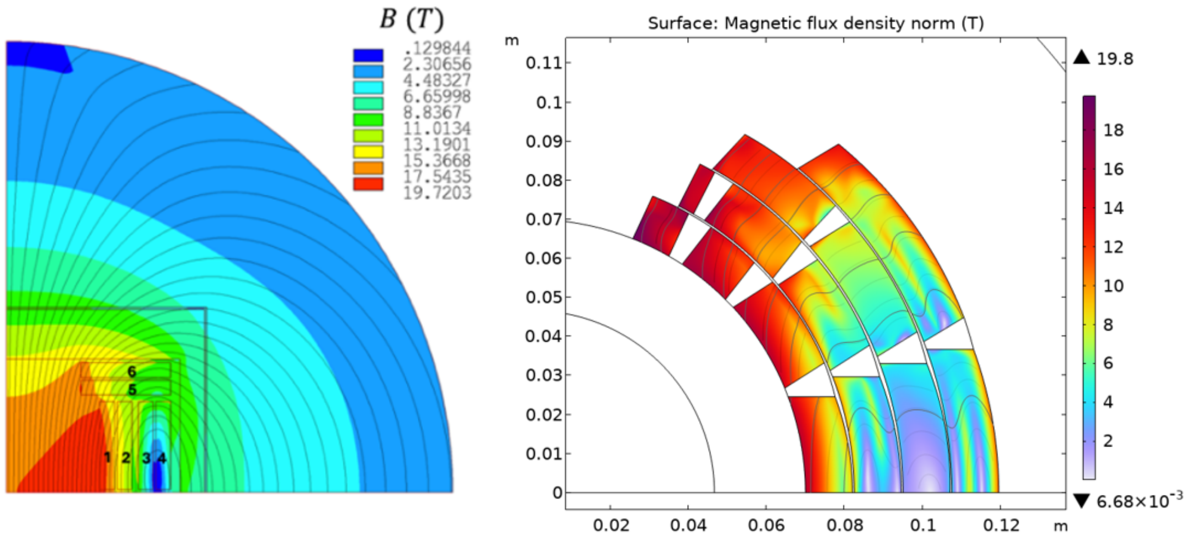

Fig. 6.1.30: Design of the cross section of HTS dipoles.

in accelerator-grade superconducting magnets. So far we have not considered Nb3Sn, which is the main focus of the High Field Magnet R&D programme, nor Nb-Ti, which is industrially available magnet technology.

Two dipole geometries are considered for this work, blocks and cos-theta. Figure M9 shows the preliminary cross sections design of the most promising candidate configurations for HTS dipole to be implemented in the ARC cell of the collider. For both configurations, a non-twisted stacked tapes cable, co-wound with a stainless steel strip is assumed. This choice is primarily due to its ease of scaling to high currents and its flexibility in cable design. Both designs satisfy the objectives of margin and stress, though many issues such as coil winding technology, ends, joints, magnetization and loss, field quality still need to be addressed in detail.

The block coil configuration consists of three double pancakes with a hybrid cable arrangement: in the four blocks on the magnet mid-plane (1-4 in Figure M11), the broad side of the cable is parallel to the horizontal-axis, while in the racetracks above the bore aperture (5-6 in Figure M11), it is oriented vertically. This configuration minimize the need for hard-way bending of the two first double pancakes while simplifying the upper racetracks winding procedure as they are positioned above the bore. The 2D magnet cross-section electromagnetic design is entirely developed using ANSYS finite element software, with the primary objective of conducting a sensitivity analysis of the geometrical parameters to meet the requirements in accordance with the A-B plots presented above. All simulations include a circular iron yoke with a mid-plane thickness of 200 mm (the outer radius is 326.7 mm), a vertical pad with a thickness of 20 mm and a horizontal pad with a thickness of 40 mm. The cos-theta coil configuration is composed by 4 layers with a 4-4-3-2 blocks arrangement. To enhance magnetic efficiency and achieve more compact designs, the block coil is graded using a two stacked tapes cable for the blocks 3 and 4 and 4 stacked tapes cable for the blocks 1, 2, 5 and 6.

Using the same cable configuration of the block coil design without any keystoning (common in LTS cable design), each block is aligned in the cross-section to minimize the geometrical field error produced in the magnet bore area while maximizing the cable temperature margin by aligning the broad face of the tape to the magnetic flux lines. The preliminary cross-section optimization is performed in Roxie without the use of iron yoke to evaluate the maximum achievable performances of the HTS winding in agreement with the analytical evaluations previously mentioned. A grading approach is used also for the cos-theta coil configuration, using instead a 50 micron stainless steel strip for the two inner coil layers and 25 micron stainless steel strip for the two outer layers. The numerical results of the electromagnetic optimization are presented in the table below.

Parameter	Unit	Block Coil Design	Cos-theta Coil Design
Operating temperature	K	20	20
Temperature margin	K	2.5	9
Bore field	T	17.5	16
Max. peak field	T	19.7	19.3
Current	A	2481	1702
Current density	A/mm^2	383 (blocks 1-2-5-6)	546 (layer 1)-612 (layer2)
		766 (blocks 3-4)	780 (layer 3)-746 (layer 4)
No. of tapes	-	524 (blocks 1-2-3-4)	546 (layer1)-612 (layer 2)
		540 (blocks 5-6)	780 (layer 3)-746 (layer 4)
Lorentz force along x	MN/m	16.03	11.0
Lorentz force along y	MN/m	-12.13	-9.52
Stored energy	MJ/m	7.58	4.9
Inductance	H/m	2.46	3.4

Table 6.1.8: Numerical results of the electromagnetic optimization of two considered configurations.

A preliminary mechanical study has been performed using ANSYS for the block coil design and COMSOL Multiphysics for the cos-theta coil configuration, both at nominal operating current. The mechanical structure has been designed to intercept the high electromagnetic forces. So far, in the evaluation of the maximum stresses in the conductors we did not consider contributions from assembly (e.g. pre-load), cool-down effects and energization phase. For this first estimation, an assumption of an ideal, infinitely rigid structure surrounding the coils is made, meaning zero nodal displacements are imposed on this element. To avoid over-constraining the conductors, and to obtaini more realistic results, a gap of 0.3 mm is maintained between the infinitely rigid structure and each pancake of the block coil design, with standard frictionless contact type applied between different elements. Since the blocks structure is considered infinitely rigid, the thickness of the infinitely rigid ribs and cases is selected arbitrarily and the definition of material and mechanical properties of the structure is not relevant. For the cos-theta coil configuration a similar infinitely rigid domain boundary condition is applied to the collars surrounding the winding to evaluate the maximum stresses on the conductor under Lorentz Forces. Each layer is considered as independent, with a frictionless contact applied to the inter-layer boundary. For both coil configurations a Young's modulus of E=174 GPa and Poisson's ratio of $\nu = 0.3$ has been considered for the conductors. The results of the preliminary mechanical simulations are shown in Figure M13.

For the block coil design, we have reported the third principal stress, which closely matches the stress distribution along the y-axis for the lower four blocks and the stress distribution along x-axis for the upper racetracks (QUESTION – what does this mean ?). For the cos-theta magnet design, the azimuthal stress on the conductor is reported for comparison.

All maximum stress values evaluated are within the maximum allowable compressive stress of 400 MPa for ReBCO tape along the direction perpendicular to the broad face. In the block coil design,

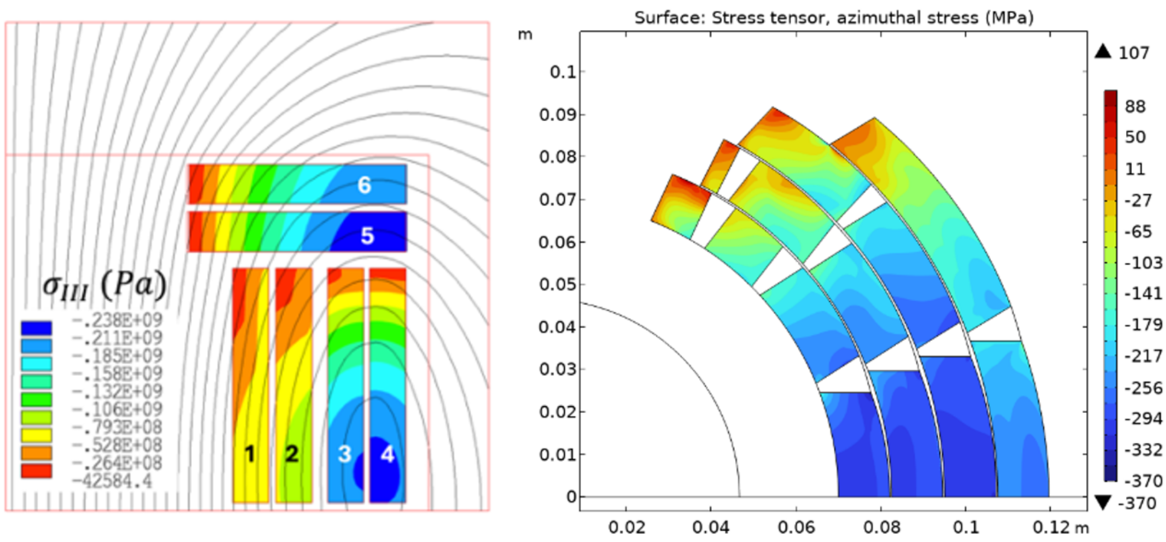

Fig. 6.1.31: Mechanical stress on conductor under Lorentz Forces at nominal current for both block coil and cos-theta magnet configurations.

the compressive stress perpendicular to the narrow face of the tape remains below 100 MPa. For the cos-theta coil configuration, a dedicated stress management strategy will be developed and implemented to mitigate radial stress accumulation on the coil, to avoid degradation of the conductor performance.

One of the issues of REBCO tapes to be understood and addressed is the effect of screening currents on field and AC loss. This is a complex matter, involving multi-physics phenomena. We are participating to the wider efforts to advance understanding and test solutions, but it will take time before accepted design methods and relevant experience are accumulated. This is why in parallel we have initiated evaluation of hysteresis losses in REBCO coils using different analytical and numerical approaches to obtain bounds. We report here first results of this work in progress.

For the block coil design we have performed an estimate of hysteresis loss using the Bean's critical state model. The evaluation assumes complete penetration of the magnetic field (corresponding to the full saturation of each tape in the model) and the field oriented perpendicular to the broad face of the tape. This approach overestimates the losses for the ramping phase by neglecting field penetration and shielding, and represents therefore a worst case-scenario. The losses per unit length due to the magnet ramping without the contribution of the transport current are (for the entire cross section) Q/L=528 KJ/m per ramp. Considering also the contribution of the transport current they increase to Q/L=652 KJ/m per ramp. These values are high, indicating that we need to dwell in finer level of detail.

To demonstrate how to improve on the above estimate, we report below the results of a calculation performed for the cos-theta coil configuration using a MATLAB optimization routine based on the Brandt Hysteresis Model [341]. The routines compute the current density distribution within HTS tapes, and the resulting hysteretic losses in the coil. The calculated current density profile for each HTS tape is driven by the external field change, but also incorporates the effect of the superconductor layer magnetization and of the transport current at each step of the magnet powering cycle. Figure M12 illustrates the redistribution of current density within the cross-section's superconducting tapes. The saturation of the outer layers, caused by the transport current, becomes evident at high operating current levels, while the inner layers remain unsaturated, continuing to contribute to the coil's hysteretic losses. (QUESTION:

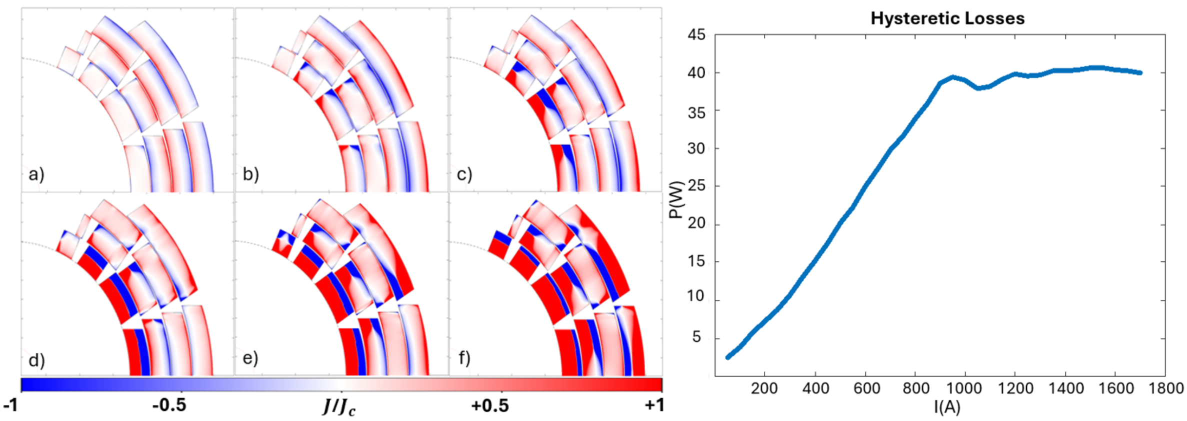

Fig. 6.1.32: Distribution of the current density in the coil cross-section at different step of the powering cycle and corresponding hysteretic losses profile as function of the magnet operating current.

why are losses decreasing around 900 A ?). The hysteresis losses during magnet operation up to the nominal current were found to reach a value of Q/L=34.8 kJ/m. This is more than an order of magnitude lower than the analytic estimate described above, and is not far from values that could be acceptable for magnet ramp to nominal. There is clearly more work to be done, but as demonstrated here we have methods and indications on how to improve the design.

6.1.0.21 Challenges identified

The challenges of the muon collider magnets, based on any of the possible technology discussed above, are driven by the combination of field (or gradient) and large apertures. Nb-Ti is an exception, as solutions for large aperture magnets of field in the range of 5 T are readily available (e.g. the HL-LHC D1 magnet). Indeed, comparing the magnet specifications set earlier to the state-of-the-art and on-going developments for both Nb3Sn and REBCO, it is evident that the magnet performance targeted is well above what has been achieved and planned so far. Still, we can profit from the fact that the lower center-of-mass collision energy required for the Muon Collider translates directly into a shorter collider ring. We can thus allow a higher cost per unit length, compared to other collider options, and design for larger coils, with more superconducting material, enabling higher dipole magnet performances, pushing the limits of magnet design.

Besides the field reach and aperture demands, both Nb3Sn and REBCO share the difficulty of:

- Managing large forces and stress, whereby REBCO has an advantage because of the higher resilience to compressive transverse stress and longitudinal tensile stress;
- Quench protection of magnets with large stored energy, where again REBCO may have the advantage of winding magnets using the non-insulated technology which, although to be demonstrated, may open the way for a next step for accelerator magnets;
- Cost. Any engineering solution needs to be affordable to scale up to the required series production of accelerator magnets, which calls for compact coils making the best use of the minimum amount of material.

Demonstrators will be necessary in any of the selected technologies. In addition, REBCO accelerator magnets will need to address:

- The issues originating from the large shielding currents: AC loss during ramps, field distortions, and internal stresses developed as the current distribution changes inside a tape;
- Coil ends and terminations, which still remain a delicate region, and for which winding shape optimization studies, development and tests are required.

6.2 Power converters

F. BOATTINI, M. GAST, D. FAZIOLI **(4-6 pages)**

Power converters for the muon accelerator

Quick acceleration is made possible by the significant electrical power supplied by the power converters. The high $\frac{dB}{dt}$ values are associated with large voltage swings according to the total impedance of the magnets that are to be powered. Concerning dipoles and quadrupole pulsed magnets, they could be connected together in series and powered by the same power converters with the Quadrupoles having an additional fast trim converter to be able controlling the tune as illustrated in Figure 6.2.1.

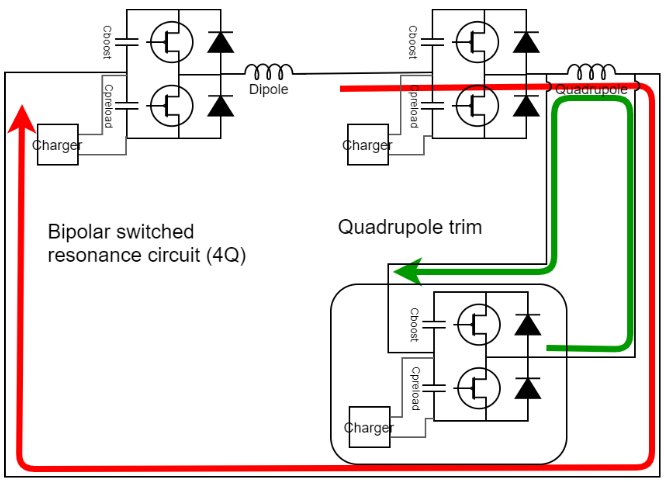

Fig. 6.2.1: Possible quadrupole powering concept

Quadrupoles will not be considered in this paragraph as they should not contribute much to the total impedance of the power converter. In the remainder of this chapter, the load will be constituted by the resistive pulsed dipole magnets only. According to the preliminary dipole magnets design shown in the magnets section, the typical impedance per meter and peak current values for the dipole magnets are:

$$L_{dipole} \approx 100\,\mu\mathrm{H/m}, \quad R_{dipole} \approx 650\,\mu\Omega/\mathrm{m}, \quad I_{\mathrm{pk}_{dipole}} \approx 11000\,\mathrm{A}$$

When computing the correspondent peak voltages and powers that the power converters must provide, we get the figures reported in Table 6.2.1 and Table 6.2.2.

To handle both high power and voltage demands, the power converters of the RCS utilize pulsed resonant circuits, such as the full-wave and two switched resonance types illustrated in Figure 6.2.2 Both circuits are based on pre-charging one or more capacitor to a convenient initial voltage and the activating a switch to discharge them. As the load is, almost, purely inductive, the capacitors will be recharged